Springer

Acta Mechanica Sinica

CrossMark click for updates

• RESEARCH PAPER •

Acta Mech. Sin., Vol. 41, 423548 (2025)
https://doi.org/10.1007/s10409-024-23548-x

Symplectic solutions for orthotropic micropolar plane stress problem

Long Chen, Zhaofei Tang, Qiong Wu, and Qiang Gao*

State Key Laboratory of Structural Analysis, Optimization and CAE Software for Industrial Equipment, Department of Engineering Mechanics, Faculty of Vehicle Engineering and Mechanics, Dalian University of Technology, Dalian 116024, China

Received November 1, 2023; accepted April 2, 2024; published online August 22, 2024

The symplectic approach was utilized to derive solutions to the orthotropic micropolar plane stress problem. The Hamiltonian canonical equation was first obtained by applying Legendre's transformation and the Hamiltonian mixed energy variational principle. Then, by using the method of separation of variables, the eigenproblem of the corresponding homogeneous Hamiltonian canonical equation was derived. Subsequently, the corresponding eigensolutions for three kinds of homogeneous boundary conditions were derived. According to the adjoint symplectic orthogonality of the eigensolutions and expansion theorems, the solutions to this plane stress problem were expressed as a series expansion of these eigensolutions. The numerical results for the orthotropic micropolar plane stress problem under various boundary conditions were presented and validated using the finite element method, which confirmed the convergence and accuracy of the proposed approach. We also investigated the relationship between the size-dependent behaviour and material parameters using the proposed approach. Furthermore, this approach was applied to analyze lattice structures under an equivalent micropolar continuum approximation.

Symplectic approach, Micropolar, Orthotropic materials, Size effect, Analytical solution

Citation: L. Chen, Z. Tang, Q. Wu, and Q. Gao, Symplectic solutions for orthotropic micropolar plane stress problem, Acta Mech. Sin. 41, 423548 (2025), https://doi.org/10.1007/s10409-024-23548-x

1. Introduction

With the development of the microelectronics technology, the use of microstructures has become increasingly prevalent [1-3], and many microstructures such as joints, cracks, and voids can be found in composite structures [4]. Some studies [5-7] have shown that the mechanical properties of structures undergo significant changes when the characteristic size approaches the micron level, resulting in a size-dependent behaviour.

According to the classical elasticity theory, the constitutive relations of structures do not incorporate the characteristic length, and microelement surfaces only transmit forces without transmitting couples. Therefore, materials containing microstructures do not exhibit size effects within the framework of the classical elasticity theory [8]. To predict the size-dependent behaviour of a material, Eringen [9,10] proposed the micropolar theory, which assumes that the microstructure can rotate independently of the surrounding medium. Owing to the incorporation of microstructures in the modelling process, the theory can correctly describe the size effect. Consequently, the micropolar theory has garnered significant attention and found extensive applications in the mechanical analysis of actual microstructures. Sargsyan and Sargsyan [11] utilized the micropolar theory to establish a dynamic mathematical model for geometrically nonlinear micropolar elastic thin plates and solved the free vibration problems of rectangular plates, circular plates, and shallow shells based on this model. Zhu et al. [12] developed a smoothed particle hydrodynamics code based on the micropolar theory, which proved effective in addressing problems involving large deformations and localized shear strain. Alemi and Shodja [5] introduced the concept of an eigencurvature field into the

*Corresponding author. E-mail address: qgao@dlut.edu.cn (Qiang Gao)
Executive Editor: Shujuan Hou

micropolar theory and discussed the influence of the characteristic size on micro- and nanoscale structures. Grbčić et al. [13] developed quadrilateral finite elements using linked interpolation within the framework of micropolar continuum theory. Berkache et al. [14] studied the effective elastic properties and mode I elastic fracture based on the micropolar continuum and found that micropolar effects are evident in the bending structure.

Despite the development of the micropolar theory, only a few papers have published analytical solutions for micropolar elastic materials. Grigor'ev and Gavrilieva [15] derived analytical solutions for a plane static problem within the framework of the micropolar theory when the normal stresses, tangential components of displacements, and couple stresses are specified on a boundary. Levin et al. [16] obtained exact analytical solutions for the problem of biaxial loading by considering micropolar and nonlinear effects. Matrosov [17] obtained an exact analytical solution for a freely supported micropolar rectangle based on the method of initial functions for a micropolar medium under plane strain conditions. Carrera and Zozulya [18] developed an analytical form Navier solution for micropolar cylindrical shell based on the Carrera unified formulation approach. Dehbani et al. [19] presented an analytical solution for functionally graded materials hollow cylinder which is micropolar magneto-thermoelasticity by using the complex Fourier series and the power-law functions. Rizzi et al. [20] derived the analytical solutions for the uniaxial extension problem within the framework of the micromorphic continuum.

The general methods used to predict the structural response of micropolar materials include numerical models and solution methods, particularly the finite element method (FEM) [17,21]. Sachio et al. [22] developed a displacement-based finite element analysis method using the total potential energy for anisotropic micropolar linear elastic materials and demonstrated the dependence of the stress concentration factor on the micropolar material parameters based on this method. Melaibari et al. [23] obtained the three-dimensional (3D) homogeneous elastic properties of orthotropic materials and analyzed the mechanical properties of orthotropic laminated structures through experiments and FEM. Huang et al. [24] proposed a new homogenization method for homogeneous and conformal metamaterials with orthogonal lattices based on FEM within the framework of the orthogonal micropolar continuum. Yang and Liu [25] constructed a finite element model for coupled stress microplates to analyze the free vibration properties of composite laminated microplates composed of orthotropic plies. Moreover, other approaches, such as the expansion theorem [26,27], asymptotic homogenization approach [28], and polynomial approximation [29,30], have also been used to analyze microstructures based on the micropolar elasticity theory.

Inspired by the analogy relationship between computational structural mechanics and modern control theory [31,32], Zhong [33,34] applied the symplectic approach to elasticity. Based on the symplectic approach, Yao and Yang [35] presented Saint-Venant solutions for multi-layered problems. Xu et al. [36] obtained the analytical solution of the vibration behavior of single-layer graphene sheets based on a nonlocal continuum orthotropic plate model within the Hamiltonian system. Qiu and Xia [37] solved the structural dynamic response with damping based on the non-conservative linear Hamiltonian system. Xu et al. [38] presented a symplectic method for analyzing fracture in two-dimensional viscoelastic media. Su et al. [39,40] used symplectic superposition and symplectic methods to derive analytical solutions for the free vibration problem of orthotropic rectangular thin plates on a two-parameter elastic foundation. Xu et al. [41] conducted a buckling analysis of a partially or internally cracked natural fiber-reinforced composite plate using the symplectic elasticity method. Further research on symplectic elasticity can be found in Ref. [42]. Recently, the symplectic approach was applied to solve problems related to size effects. Luo et al. [43] proposed a new state vector formulation for a 3D couple stress problem based on the symplectic approach. Shaw [44] analyzed the dynamics of rectangular micropolar beams in the high-frequency domain using the symplectic approach. Xu et al. [45] used the symplectic approach to investigate the influence of the size and in-plane magnetic field on the free vibration of a double-layered nanoplate system.

In this study, the analytical solutions for the orthotropic micropolar plane stress problem were obtained, which is difficult to derive using the classical approach by a semi-inverse method due to the complexity of the material parameters and boundary conditions. First, the Hamiltonian canonical equation was derived using Legendre's transformation and the Hamiltonian mixed energy variational principle. Subsequently, using the method of separation of variables, the homogeneous Hamiltonian canonical equation was transformed into an eigenproblem of the Hamiltonian operator matrix. The corresponding eigensolutions for three types of homogeneous boundary conditions at both side edges were then determined. Finally, based on the adjoint symplectic orthogonal relation of the eigensolutions, the general solution to the original problem was expressed as a series expansion of the eigensolutions. Additionally, the relationship between the size-dependent behaviour and material parameters for the orthotropic microplate plane stress problem was investigated, and the proposed method was applied to analyze lattice structures under an equivalent micropolar continuum approximation.

The remainder of this paper is organized as follows. In Sect. 2, the fundamental equations of the orthotropic micropolar plane stress problem are briefly reviewed. Then, the derivation of the Hamiltonian canonical equation based

on Legendre's transformation and the Hamiltonian mixed energy variational principle is detailed in Sect. 3. In Sect. 4, the derivation of the corresponding eigensolutions for the three types of homogeneous boundary conditions at both side edges are described. Section 5 obtained the solutions of the orthotropic micropolar plane stress problem according to the symplectic eigen expansion. In Sect. 6, the numerical results are presented to demonstrate the validity and accuracy of the proposed approach.

2. Fundamental equations of an orthotropic micropolar plane stress problem

An orthotropic rectangular microplate with length L, width $2h$, and thickness δ is shown in Fig. 1, where the x-axis is the longitudinal coordinate in a Cartesian coordinate system. According to the linear theory of micropolar elasticity, the geometric equations of the microplate are as follows [46]:

$$\begin{aligned}&\varepsilon_{xx}=\frac{\partial u}{\partial x},\ \varepsilon_{yy}=\frac{\partial v}{\partial y},\ \gamma_{xy}=\frac{\partial v}{\partial x}-\theta,\\&\gamma_{yx}=\frac{\partial u}{\partial y}+\theta,\ \chi_{xz}=\frac{\partial \theta}{\partial x},\ \chi_{yz}=\frac{\partial \theta}{\partial y},\end{aligned}\tag{1}$$

where ε_{xx}, ε_{yy}, γ_{xy}, and γ_{yx} are the strains; χ_{xz} and χ_{yz} are the curvatures; u and v are the in-plane displacements; and θ is the out-of-plane microrotation. For orthotropic micropolar continuous materials, the constitutive equations for the plane stress condition are [22]

$$\begin{aligned}&\sigma_{xx}=\frac{E_1}{1-\nu_{12}\nu_{21}}\left(\varepsilon_{xx}+\nu_{21}\varepsilon_{yy}\right),\\&\sigma_{yy}=\frac{E_2}{1-\nu_{12}\nu_{21}}\left(\varepsilon_{yy}+\nu_{12}\varepsilon_{xx}\right),\\&\tau_{xy}=\frac{G}{1-N^2}\left[\gamma_{xy}+(1-2N^2)\gamma_{yx}\right],\\&\tau_{yx}=\frac{G}{1-N^2}\left[\gamma_{yx}+(1-2N^2)\gamma_{xy}\right],\\&m_{xz}=4Gl_x^2\chi_{xz},\ m_{yz}=4Gl_y^2\chi_{yz},\end{aligned}\tag{2}$$

where σ_{xx}, σ_{yy}, τ_{xy}, and τ_{yx} are the stresses; m_{xz} and m_{yz} are the couple stresses; N is the coupling factor; l_x and l_y are the characteristic lengths; G is the shear modulus; E_1 and E_2 are the Young's moduli along the x and y directions, respectively; ν_{12} is the Poisson's ratio describing the constriction in the y direction due to stretching in the x direction; ν_{21} has an analogous meaning except that y and x are interchanged; and the Young's modulus and Poisson's ratio obey the following property: $E_1\nu_{21}=E_2\nu_{12}$. The equilibrium equations for this problem are as follows:

$$\begin{aligned}&\frac{\partial \sigma_{xx}}{\partial x}+\frac{\partial \tau_{yx}}{\partial y}+f_x=0,\ \frac{\partial \sigma_{yy}}{\partial y}+\frac{\partial \tau_{xy}}{\partial x}+f_y=0,\\&\frac{\partial m_{xz}}{\partial x}+\frac{\partial m_{yz}}{\partial y}+\tau_{xy}-\tau_{yx}+m_z=0,\end{aligned}\tag{3}$$

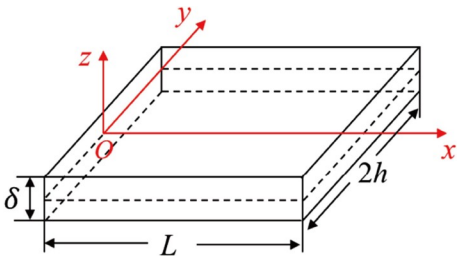

Figure 1 Schematic illustration of the micropolar plate and coordinate system.

where f_x and f_y are the body forces and m_z is the body couple. The boundary conditions can be expressed as follows:

$$\begin{aligned}&\sigma_{xx}n_x+\sigma_{yy}n_y=\bar{\sigma}\quad\text{or}\quad u=\bar{u},\\&\tau_{xy}n_x+\tau_{yx}n_y=\bar{\tau}\quad\text{or}\quad v=\bar{v},\\&m_{xz}n_x+m_{yz}n_y=\bar{m}\quad\text{or}\quad \theta=\bar{\theta},\end{aligned}\tag{4}$$

where n_x and n_y denote the direction cosine of the unit normal vector with respect to the x- and y-axes on the boundary, respectively; $\bar{\sigma}$, $\bar{\tau}$, and $\bar{m}$ are the specified forces and couple force, respectively; and $\bar{u}$, $\bar{v}$, and $\bar{\theta}$ are the applied displacements and microrotation, respectively.

3. Hamiltonian canonical equations for an orthotropic micropolar plane stress problem

To solve the orthotropic micropolar plane stress problem in a Hamiltonian system, the Lagrange density function is first defined as [47]

$$L=U_\varepsilon-uf_x-vf_y-\theta m_z,\tag{5}$$

where the strain energy U_ε is

$$U_\varepsilon=\frac{1}{2}\left(\sigma_{xx}\varepsilon_{xx}+\sigma_{yy}\varepsilon_{yy}+\tau_{xy}\varepsilon_{xy}+\tau_{yx}\varepsilon_{yx}+m_{xz}\chi_{xz}+m_{yz}\chi_{yz}\right).\tag{6}$$

Substituting Eqs. (1) and (2) into Eq. (5) yields

$$L(\mathbf{q},\dot{\mathbf{q}})=\frac{1}{2}\dot{\mathbf{q}}^{\mathrm{T}}\mathbf{K}_{22}\dot{\mathbf{q}}+\dot{\mathbf{q}}^{\mathrm{T}}\mathbf{K}_{21}\mathbf{q}+\frac{1}{2}\mathbf{q}^{\mathrm{T}}\mathbf{K}_{11}\mathbf{q}-\mathbf{f}^{\mathrm{T}}\mathbf{q},\tag{7}$$

in which the dot represents differentiation with respect to x, and

$$\mathbf{q}=[u\quad v\quad \theta]^{\mathrm{T}},\quad \mathbf{f}=\left[f_x\quad f_y\quad m_z\right]^{\mathrm{T}},\tag{8}$$

$$\mathbf{K}_{22}=\begin{bmatrix}\dfrac{E_1}{1-\nu_{12}\nu_{21}} & 0 & 0\\ 0 & \dfrac{G}{1-N^2} & 0\\ 0 & 0 & 4Gl_x^2\end{bmatrix},$$

$$\mathbf{K}_{21}=\begin{bmatrix}0 & \dfrac{E_1\nu_{21}}{1-\nu_{12}\nu_{21}}\dfrac{\partial}{\partial y} & 0\\ G\dfrac{1-2N^2}{1-N^2}\dfrac{\partial}{\partial y} & 0 & -\dfrac{2GN^2}{1-N^2}\\ 0 & 0 & 0\end{bmatrix},$$

$$\mathbf{K}_{11}=\begin{bmatrix} -\dfrac{G}{1-N^2}\dfrac{\partial^2}{\partial y^2} & 0 & -\dfrac{2GN^2}{1-N^2}\dfrac{\partial}{\partial y} \\ 0 & -\dfrac{E_2}{1-\nu_{12}\nu_{21}}\dfrac{\partial^2}{\partial y^2} & 0 \\ \dfrac{2GN^2}{1-N^2}\dfrac{\partial}{\partial y} & 0 & \dfrac{4GN^2}{1-N^2}-4Gl_y^2\dfrac{\partial^2}{\partial y^2} \end{bmatrix}, \tag{9}$$

where $\mathbf{K}_{22}$ is a diagonal matrix; $\mathbf{K}_{21}$ is an operator matrix; and $\mathbf{K}_{11}$ is a symmetric operator matrix.

Applying Legendre's transformation [35] to Eq. (7) yields the dual vector $\mathbf{p}$ of the displacement vector $\mathbf{q}$, that is

$$\mathbf{p}=\frac{\partial L(\mathbf{q},\dot{\mathbf{q}})}{\partial\dot{\mathbf{q}}}=\mathbf{K}_{22}\dot{\mathbf{q}}+\mathbf{K}_{21}\mathbf{q}. \tag{10}$$

It can be proved that

$$\mathbf{p}=\begin{bmatrix}\sigma_{xx} & \tau_{xy} & m_{xz}\end{bmatrix}^{\mathrm{T}}. \tag{11}$$

Eq. (10) can be rewritten as

$$\dot{\mathbf{q}}=-\mathbf{K}_{22}^{-1}\mathbf{K}_{21}\mathbf{q}+\mathbf{K}_{22}^{-1}\mathbf{p}. \tag{12}$$

Subsequently, the Hamiltonian density function is introduced as

$$H(\mathbf{q},\mathbf{p})=\mathbf{p}^{\mathrm{T}}\dot{\mathbf{q}}-L(\mathbf{q},\dot{\mathbf{q}}). \tag{13}$$

Substituting Eqs. (7) and (12) into Eq. (13) yields

$$H(\mathbf{q},\mathbf{p})=-\mathbf{p}^{\mathrm{T}}\mathbf{A}\mathbf{q}-\frac{1}{2}\mathbf{q}^{\mathrm{T}}\mathbf{B}\mathbf{q}+\frac{1}{2}\mathbf{p}^{\mathrm{T}}\mathbf{D}\mathbf{p}+\mathbf{f}^{\mathrm{T}}\mathbf{q}, \tag{14}$$

in which

$$\mathbf{A}=\mathbf{K}_{22}^{-1}\mathbf{K}_{21},\quad \mathbf{B}=\mathbf{K}_{11}-\mathbf{K}_{21}^{\mathrm{T}}\mathbf{K}_{22}^{-1}\mathbf{K}_{21},\quad \mathbf{D}=\mathbf{K}_{22}^{-1}. \tag{15}$$

Here, the transpose of an operator matrix is an adjoint operator matrix rather than a simple transposition. Because $\mathbf{K}_{11}$ is a symmetric operator matrix; $\mathbf{K}_{21}$ is an operator matrix; $\mathbf{K}_{22}$ is a diagonal matrix; $\mathbf{A}$ is an operator matrix; $\mathbf{B}$ is a symmetric operator matrix; and $\mathbf{D}$ is a diagonal matrix. Through the above derivation, the displacements u, v, and θ as well as stresses σ_{xx}, τ_{xy}, and m_{xz} are defined as mutual dual vectors $\mathbf{q}$ and $\mathbf{p}$ in the symplectic space, respectively. To facilitate the following derivation, the stresses σ_{yy}, τ_{yx}, and m_{yz} are expressed by the mutual dual vectors $\mathbf{q}$ and $\mathbf{p}$, that is

$$\mathbf{b}=\mathbf{L}_1\mathbf{q}+\mathbf{L}_2\mathbf{p}, \tag{16}$$

in which

$$\mathbf{b}=\begin{bmatrix}\tau_{yx} & \sigma_{yy} & m_{yz}\end{bmatrix}^{\mathrm{T}}, \tag{17}$$

$$\mathbf{L}_1=\begin{bmatrix} 4GN^2\dfrac{\partial}{\partial y} & 0 & 4GN^2 \\ 0 & E_2\dfrac{\partial}{\partial y} & 0 \\ 0 & 0 & 4Gl_y^2\dfrac{\partial}{\partial y} \end{bmatrix},\quad \mathbf{L}_2=\begin{bmatrix} 0 & 1-2N^2 & 0 \\ \nu_{21} & 0 & 0 \\ 0 & 0 & 0 \end{bmatrix}. \tag{18}$$

Next, the Hamiltonian mixed energy variational principle is applied to derive the Hamiltonian dual equation and corresponding boundary conditions. For the micropolar planar plate, different boundary conditions exist at each edge, and the derivations under different boundary conditions are similar. Thus, the boundary condition in which the specified stresses are applied on edges $y=\pm h$ and $x=0$ and the specified displacements are applied on edge $x=L$, is taken as an example to show the derivation.

Using the Hamiltonian density function defined in Eq. (14), the Hamiltonian mixed energy variational principle can be expressed as

$$\delta\left\{\int_0^L\int_{-h}^{h}[p^{\mathrm{T}}\dot{\mathbf{q}}-H(\mathbf{q},\mathbf{p})]\mathrm{d}y\mathrm{d}x-\int_0^L\left[\left(\bar{\mathbf{b}}_1^{\mathrm{T}}\mathbf{q}\right)_{y=h}-\left(\bar{\mathbf{b}}_2^{\mathrm{T}}\mathbf{q}\right)_{y=-h}\right]\mathrm{d}x \right.$$
$$\left.-\int_{-h}^{h}[\mathbf{p}^{\mathrm{T}}(\mathbf{q}-\bar{\mathbf{q}})]_{x=L}\mathrm{d}y-\int_{-h}^{h}(\bar{\mathbf{p}}^{\mathrm{T}}\mathbf{q})_{x=0}\mathrm{d}y\right\}=0, \tag{19}$$

in which $\bar{\mathbf{p}}$ are the prescribed stresses at edge $x=0$, $\bar{\mathbf{q}}$ are the specified displacements at edge $x=L$, $\bar{\mathbf{b}}_1$ are the prescribed stresses at edge $y=h$, and $\bar{\mathbf{b}}_2$ are the prescribed stresses at edge $y=-h$. Implementing the variation in Eq. (19) yields the following dual equation:

$$\dot{\mathbf{v}}=\mathbf{H}\mathbf{v}+\mathbf{h}, \tag{20}$$

in which the full state vector $\mathbf{v}$ is

$$\mathbf{v}=[\mathbf{q}\quad \mathbf{p}]^{\mathrm{T}}, \tag{21}$$

and

$$\mathbf{H}=\begin{bmatrix}-\mathbf{A} & \mathbf{D} \\ \mathbf{B} & \mathbf{A}^{\mathrm{T}}\end{bmatrix},\quad \mathbf{h}=[\mathbf{0}\quad -\mathbf{f}]^{\mathrm{T}}. \tag{22}$$

After applying the variation in Eq. (19), the boundary conditions at edges $y=\pm h$ can be obtained as

$$\mathbf{L}_1\mathbf{q}+\mathbf{L}_2\mathbf{p}=\bar{\mathbf{b}}_1,\ y=h,\ \mathbf{L}_1\mathbf{q}+\mathbf{L}_2\mathbf{p}=\bar{\mathbf{b}}_2,\ y=-h, \tag{23}$$

and the boundary conditions at both ends $x=0$, L can be expressed as

$$\mathbf{p}=\bar{\mathbf{p}},\quad x=0,\quad \mathbf{q}=\bar{\mathbf{q}},\quad x=L. \tag{24}$$

According to Yao and Yang [35], if the boundary conditions at edges $y=\pm h$ are homogeneous and the state vector $\mathbf{v}$ satisfies these homogeneous boundary conditions, $\mathbf{H}$ is a Hamiltonian operator matrix. Hence, three types of homogeneous boundary conditions at edges $y=\pm h$ are considered in this study: free boundary, clamped boundary, and boundary conditions in which one edge is free and the other is clamped. These boundary conditions are expressed as follows:

(a) free boundary conditions

$$\mathbf{L}_1\mathbf{q}+\mathbf{L}_2\mathbf{p}=\mathbf{0},\quad y=\pm h; \tag{25}$$

(b) clamped boundary conditions

$$\mathbf{q}=\mathbf{0},\quad y=\pm h; \tag{26}$$

(c) boundary conditions where the edge at $y=h$ is free

and that at $y=-h$ is clamped

$$\mathbf{L}_1\mathbf{q}+\mathbf{L}_2\mathbf{p}=\mathbf{0}, \quad y=h, \quad \mathbf{q}=\mathbf{0}, \quad y=-h. \tag{27}$$

4. Eigensolutions for homogeneous Hamiltonian canonical equation

4.1 Method of separation of variables

To solve the Hamiltonian dual equation in Eq. (20), the corresponding homogeneous linear differential equation

$$\dot{\mathbf{v}}=H\mathbf{v} \tag{28}$$

should be solved in advance. Applying the method of separation of variables to the full state vector $\mathbf{v}$ yields

$$\mathbf{v}(x,y)=r(x)\boldsymbol{\psi}(y), \tag{29}$$

where

$$\boldsymbol{\psi}(y)=\left[u^* \quad v^* \quad \theta^* \quad \sigma_{xx}^* \quad \tau_{xy}^* \quad m_{xz}^*\right]^{\mathrm{T}}. \tag{30}$$

Substituting Eq. (29) into Eq. (28) results in

$$r(x)=\exp(\mu x), \tag{31}$$

and the eigenvalue equation is

$$\mathbf{H}\boldsymbol{\psi}(y)=\mu\boldsymbol{\psi}(y), \tag{32}$$

where μ is the eigenvalue and $\boldsymbol{\psi}(y)$ is the eigenvector. Because the zero eigenvalue is a special eigenvalue in the Hamiltonian eigenproblem, and the eigensolutions of this eigenvalue contain a specific physical meaning in elasticity [34], the eigenvalues are categorized into two groups, namely zero eigenvalues and nonzero eigenvalues, which are presented in Sect. 4.

4.2 Eigensolutions for the free boundary conditions at $y=\pm h$

4.2.1 *Zero eigenvalue solutions*

In the Hamiltonian eigenvalue problem, when the boundary conditions at edges $y=\pm h$ are free, repeated zero eigenvalues and the corresponding various orders of Jordan form eigenvectors exist [33]. Substituting $\mu=0$ into Eq. (32) yields

$$\mathbf{H}\boldsymbol{\psi}(y)=0. \tag{33}$$

By solving Eq. (33) using Eq. (25), the fundamental eigenvectors are determined as follows:

$$\boldsymbol{\psi}_{01}^{(0)}=[1 \quad 0 \quad 0 \quad 0 \quad 0 \quad 0]^{\mathrm{T}}, \tag{34}$$

$$\boldsymbol{\psi}_{02}^{(0)}=[0 \quad 1 \quad 0 \quad 0 \quad 0 \quad 0]^{\mathrm{T}}, \tag{35}$$

where the superscript 0 denotes the 0-th order Jordan form (basic) eigenvector, and the subscript 0 represents the eigenvectors of zero eigenvalue. There are two chains denoted by subscripts 1 and 2.

The governing equation of the i-th Jordan form eigenvector of zero eigenvalue can be written as

$$\mathbf{H}\boldsymbol{\psi}_{0j}^{(i)}=\boldsymbol{\psi}_{0j}^{(i-1)} \quad (i=1,2,\cdots,n;\ j=1,2). \tag{36}$$

Solving $\mathbf{H}\boldsymbol{\psi}_{01}^{(1)}=\boldsymbol{\psi}_{01}^{(0)}$ and $\mathbf{H}\boldsymbol{\psi}_{02}^{(1)}=\boldsymbol{\psi}_{02}^{(0)}$ using the free boundary conditions in Eq. (25) yields the first-order Jordan form eigenvectors of chains 1 and 2 as

$$\boldsymbol{\psi}_{01}^{(1)}=\left[0 \quad -\nu_{12}y \quad 0 \quad E_1 \quad 0 \quad 0\right]^{\mathrm{T}}, \tag{37}$$

$$\boldsymbol{\psi}_{02}^{(1)}=\left[-y \quad 0 \quad 1 \quad 0 \quad 0 \quad 0\right]^{\mathrm{T}}. \tag{38}$$

However, there is no solution satisfying $\mathbf{H}\boldsymbol{\psi}_{01}^{(2)}=\boldsymbol{\psi}_{01}^{(1)}$ and the boundary conditions, indicating that the Jordan form eigenvector of chain 1 is terminated. Solving $\mathbf{H}\boldsymbol{\psi}_{02}^{(2)}=\boldsymbol{\psi}_{02}^{(1)}$ using Eq. (25) provides the second-order Jordan form eigenvector of chain 2

$$\boldsymbol{\psi}_{02}^{(2)}=\left[0 \quad \frac{1}{2}\nu_{12}y^2+c \quad 0 \quad -E_1y \quad 0 \quad 4Gl_x^2\right]^{\mathrm{T}}, \tag{39}$$

where the unknown constant c can be obtained using the symplectic orthogonal relation of eigenvectors. Similarly, solving $\mathbf{H}\boldsymbol{\psi}_{02}^{(3)}=\boldsymbol{\psi}_{02}^{(2)}$ using Eq. (25) yields the third-order Jordan form eigenvector of chain 2 as

$$\boldsymbol{\psi}_{02}^{(3)}=\begin{bmatrix}(2G\nu_{12}-E_1)\dfrac{l_y^2h\sinh(Ny/l_y)}{G\sinh(Nh/l_y)}-\dfrac{(G\nu_{12}-E_1)y^3}{6G}-\dfrac{E_1y\left(h^2-2l_y^2\right)}{2G}-y\left(2l_y^2\nu_{12}+2l_x^2+c\right)\\ 0\\ -(2G\nu_{12}-E_1)\dfrac{l_yhN\cosh(Ny/l_y)}{2GN^2\sinh(Nh/l_y)}+\dfrac{\nu_{12}y^2}{2}+\dfrac{E_1\left(h^2-y^2\right)}{4G}+\dfrac{l_y^2\nu_{12}+l_x^2}{N^2}-\dfrac{E_1l_y^2}{2GN^2}+c\\ 0\\ (4G\nu_{12}-2E_1)\dfrac{l_yNh\cosh(Ny/l_y)}{\sinh(Nh/l_y)}-\dfrac{\left(h^2-y^2-4l_y^2\right)E_1}{2}+4G\left(l_y^2\nu_{12}+l_x^2\right)\\ 0\end{bmatrix}. \tag{40}$$

There is no solution when solving $\mathbf{H}\boldsymbol{\psi}_{02}^{(4)}=\boldsymbol{\psi}_{02}^{(3)}$ using Eq. (25); thus, the Jordan form eigenvector of chain 2 is terminated.

Finally, the unknown constant c in Eqs. (39) and (40) can be obtained using the symplectic orthogonal relation of $\boldsymbol{\psi}_{02}^{(2)}$ and $\boldsymbol{\psi}_{02}^{(3)}$ as follows:

$$\left\langle \boldsymbol{\psi}_{02}^{(2)},\boldsymbol{\psi}_{02}^{(3)}\right\rangle=\int_{-h}^{h}\left(\boldsymbol{\psi}_{02}^{(2)}\right)^{\mathrm{T}}\mathbf{J}\boldsymbol{\psi}_{02}^{(3)}\mathrm{d}y=0. \tag{41}$$

Substituting Eqs. (39) and (40) into Eq. (41) results in

$$\begin{aligned}c=&-\frac{6Gl_x^4}{N^2\left(12Gl_x^2+E_1h^2\right)}-\frac{2\left(Gh^2\nu_{12}+E_1h^2\right)l_x^2}{12Gl_x^2+E_1h^2}-\frac{3(2G\nu_{12}-E_1)^2l_x^4}{2GN^2\left(12Gl_x^2+E_1h^2\right)}\\&-\frac{3h(2G\nu_{12}-E_1)^2l_y^3}{2GN\tanh\left(Nh/l_y\right)\left(12Gl_x^2+E_1h^2\right)}+\frac{(2Gh\nu_{12}-E_1h)^2l_y^2}{2G\left(12Gl_x^2+E_1h^2\right)}-\frac{E_1(G\nu_{12}+2E_1)h^4}{10G\left(12Gl_x^2+E_1h^2\right)}.\end{aligned} \tag{42}$$

4.2.2 *Nonzero eigenvalue solutions*

The zero eigenvalue solutions are obviously incomplete in the entire solution space, and nonzero eigenvalue solutions exist, which are presented in the following derivation.

Eq. (32) can be rewritten as

$$(\mathbf{H}-\mu\mathbf{I})\boldsymbol{\psi}(y)=\mathbf{0}. \tag{43}$$

This is a system of ordinary differential equations with respect to y, which can be solved by precomputing the eigenvalue λ. The corresponding equation is

$$\begin{vmatrix}-\mu & -\nu_{21}\lambda & 0 & \frac{1-\nu_{12}\nu_{21}}{E_1} & 0 & 0\\ (2N^2-1)\lambda & -\mu & 2N^2 & 0 & \frac{1-N^2}{G} & 0\\ 0 & 0 & -\mu & 0 & 0 & \frac{1}{4Gl_x^2}\\ -4GN^2\lambda^2 & 0 & -4GN^2\lambda & -\mu & (2N^2-1)\lambda & 0\\ 0 & -E_2\lambda^2 & 0 & -\nu_{21}\lambda & -\mu & 0\\ 4GN^2\lambda & 0 & 4G\left(N^2-l_y^2\lambda^2\right) & 0 & -2N^2 & -\mu\end{vmatrix}=0. \tag{44}$$

From Eq. (44), the characteristic equation is

$$\alpha_1\lambda^6-\alpha_2\lambda^4-\alpha_3\lambda^2-\alpha_4=0, \tag{45}$$

in which

$$\begin{aligned}\alpha_1&=\frac{l_y^2\nu_{21}}{l_x^2\nu_{12}},\\ \alpha_2&=\frac{2l_y^2\nu_{21}\mu^2}{l_x^2}(2N^2-1)-\frac{\mu^2l_y^2E_2}{Gl_x^2}(N^2-1)+\frac{\nu_{21}\mu^2}{\nu_{12}}-\frac{\nu_{21}N^2}{\nu_{12}l_x^2}\\&\quad-\frac{4GN^2\mu^2l_y^2}{E_1l_x^2}(\nu_{12}\nu_{21}-1),\\ \alpha_3&=\frac{\mu^2}{l_x^2}\left[\left(l_y\mu\right)^2+2N^2\nu_{21}\right]-\frac{E_2\mu^2\left[(l_x\mu)^2(N^2-1)+N^2\right]}{Gl_x^2}\\&\quad-\frac{4G(\mu N\mu\nu_{21})^2}{E_2}+\frac{4G\mu^4N^2}{E_1}+2\nu_{21}\mu^4(2N^2-1),\\ \alpha_4&=\mu^6-\frac{N^2\mu^4}{l_x^2}.\end{aligned} \tag{46}$$

Solving Eq. (45) yields the characteristic roots λ as

$$\lambda_{1,2}=\pm\beta_1\mathrm{i},\ \lambda_{3,4}=\pm\beta_2\mathrm{i},\ \lambda_{5,6}=\pm\beta_3\mathrm{i}, \tag{47}$$

where the multiplicator $\mathrm{i}=\sqrt{-1}$ is an imaginary unit that enables the expression of a general solution in the form of a trigonometric function.

Similar to the classical elasticity [33], the general solution can be categorized into two groups: solutions of symmetric and antisymmetric deformations with respect to the x-axis. For the convenience of distinguishing these solutions, the components of the vector $\boldsymbol{\psi}(y)$ in Eq. (30) are rearranged, and the general solution is expressed as

$$\overline{\boldsymbol{\psi}}(y)=\begin{bmatrix}\mathbf{M} & \mathbf{N}\\ \mathbf{S} & \mathbf{W}\end{bmatrix}\mathbf{g}, \tag{48}$$

where

$$\begin{aligned}\overline{\boldsymbol{\psi}}(y)&=\left[u^*\quad \sigma_{xx}^*\quad v^*\quad \theta^*\quad \tau_{xy}^*\quad m_{xz}^*\right]^{\mathrm{T}},\\ \mathbf{g}&=\left[\sin(\beta_1y)\quad \sin(\beta_2y)\quad \sin(\beta_3y)\quad \cos(\beta_1y)\quad \cos(\beta_2y)\quad \cos(\beta_3y)\right]^{\mathrm{T}}.\end{aligned} \tag{49}$$

Here, **M** and **N** are 2 × 3 matrices, whereas **S** and **W** are 4 × 3 matrices. The constants in matrices **M**, **N**, **S**, and **W** are not all independent. To facilitate the expression of these relationships, we choose M_{2j} and N_{2j} ($j = 1, 2, 3$) as independent constants. Substituting Eq. (48) into Eq. (43) leads to the following relationship between these constants:

$$\begin{bmatrix}\mathbf{M}\\ \mathbf{W}\end{bmatrix} = \mathbf{U}^1\mathbf{M}_2, \quad \begin{bmatrix}\mathbf{N}\\ \mathbf{S}\end{bmatrix} = \mathbf{U}^2\mathbf{N}_2, \tag{50}$$

where

$$\mathbf{M}_2 = \begin{bmatrix} M_{21} & 0 & 0\\ 0 & M_{22} & 0\\ 0 & 0 & M_{23}\end{bmatrix}, \quad \mathbf{N}_2 = \begin{bmatrix} N_{21} & 0 & 0\\ 0 & N_{22} & 0\\ 0 & 0 & N_{23}\end{bmatrix}. \tag{51}$$

$\mathbf{U}^1$ and $\mathbf{U}^2$ are 6 × 3 matrices, whose components in the first column are expressed as

$$\begin{aligned}
U_{11}^1 &= -\frac{\mu^2(2G\nu_{12}\nu_{21} - E_2\nu_{12} - 2G) + E_2\beta_1^2}{E_1\mu\gamma_2},\\
U_{21}^1 &= 1,\\
U_{31}^1 &= \frac{\gamma_2\nu_{12} - 2G\left(\nu_{12}\mu^2 + \beta_1^2\right) + \mu^2 E_1}{E_1\beta_1\gamma_2},\\
U_{41}^1 &= \frac{\gamma_1}{2G\mu E_1 N^2\beta_1\gamma_2},\\
U_{51}^1 &= \frac{\beta_1\left[2G\nu_{21}\beta_1^2 + \mu^2\nu_{12}(2G\nu_{21} - E_2)\right]}{\mu\nu_{12}\gamma_2},\\
U_{61}^1 &= \frac{2l_x^2\gamma_1}{\beta_1 E_1 N^2\gamma_2},
\end{aligned} \tag{52}$$

$$\begin{aligned}
&U_{11}^2 = U_{11}^1,\ U_{21}^2 = 1,\ U_{31}^2 = -U_{31}^1,\\
&U_{41}^2 = -U_{41}^1,\ U_{51}^2 = -U_{51}^1,\ U_{61}^2 = -U_{61}^1,
\end{aligned} \tag{53}$$

in which

$$\begin{aligned}
\gamma_1 = {}&(\mu\beta_1)^2\left[4N^2(\nu_{12}\nu_{21} - 1)G^2 - 2G\nu_{12}E_2(2N^2 - 1)\right.\\
&\left. + E_2E_1(N^2 - 1)\right] + E_1G\mu^4 + E_2G\beta_1^4,
\end{aligned} \tag{54}$$

$$\gamma_2 = (2G\nu_{21} - E_2)\beta_1^2 + 2G\mu^2.$$

The expressions of the components in the other two columns of matrices $\mathbf{U}^1$ and $\mathbf{U}^2$ are analogous to those in the first column, except that β_1 is replaced with β_2 and β_3, respectively.

Because the free boundary conditions at $y = \pm h$ are symmetric with respect to the x-axis, according to Eq. (48), the general solution for the symmetric deformation is

$$\overline{\boldsymbol{\psi}}_{\mathrm{s}}(y) = \begin{bmatrix}\mathbf{0} & \mathbf{N}\\ \mathbf{S} & \mathbf{0}\end{bmatrix}\mathbf{g}, \tag{55}$$

and that for the antisymmetric deformation is

$$\overline{\boldsymbol{\psi}}_{\mathrm{a}}(y) = \begin{bmatrix}\mathbf{M} & \mathbf{0}\\ \mathbf{0} & \mathbf{W}\end{bmatrix}\mathbf{g}. \tag{56}$$

For the symmetric deformation, substituting Eqs. (55) and (50) into Eq. (25) yields

$$\mathbf{V}^{\mathrm{f}}\mathbf{C}_{\mathrm{s}} = \mathbf{0}, \tag{57}$$

in which

$$\mathbf{C}_{\mathrm{s}} = \begin{bmatrix} N_{21} & N_{22} & N_{23}\end{bmatrix}^{\mathrm{T}}. \tag{58}$$

Here, the components of the coefficient matrix $\mathbf{V}^{\mathrm{f}}$ are expressed as

$$\begin{aligned}
V_{11}^{\mathrm{f}} &= \frac{\mu^2\nu_{12}(2G\nu_{21} - E_2) + 2G\nu_{21}\beta_1^2}{\nu_{12}\gamma_2}\cos(\beta_1 h),\\
V_{21}^{\mathrm{f}} &= -\frac{\sin(\beta_1 h)\mu}{\beta_1}, \quad V_{31}^{\mathrm{f}} = -\frac{2l_y^2\cos(\beta_1 h)\gamma_1}{E_1N^2\mu\gamma_2}.
\end{aligned} \tag{59}$$

The expressions for V_{m2}^{f} and V_{m3}^{f} ($m = 1, 2, 3$) are analogous to those for V_{m1}^{f}, with the only difference being the substitution of β_1 with β_2 and β_3, respectively.

For the antisymmetric deformation, substituting Eqs. (56) and (50) into Eq. (25) yields

$$\mathbf{R}^{\mathrm{f}}\mathbf{C}_{\mathrm{a}} = \mathbf{0}, \tag{60}$$

in which

$$\mathbf{C}_{\mathrm{a}} = \begin{bmatrix} M_{21} & M_{22} & M_{23}\end{bmatrix}^{\mathrm{T}}. \tag{61}$$

Here, the components of the coefficient matrix $\mathbf{R}^{\mathrm{f}}$ are expressed as

$$\begin{aligned}
R_{11}^{\mathrm{f}} &= \frac{\mu^2\nu_{12}(2G\nu_{21} - E_2) + 2G\nu_{21}\beta_1^2}{\nu_{12}\gamma_2}\sin(\beta_1 h),\\
R_{21}^{\mathrm{f}} &= \frac{\cos(\beta_1 h)\mu}{\beta_1}, \quad R_{31}^{\mathrm{f}} = -\frac{2l_y^2\sin(\beta_1 h)\gamma_1}{E_1N^2\mu\gamma_2}.
\end{aligned} \tag{62}$$

The expressions for R_{m2}^{f} and R_{m3}^{f} ($m = 1, 2, 3$) are analogous to those for R_{m1}^{f}, except that β_1 is replaced with β_2 and β_3, respectively.

To obtain the nontrivial solutions to Eqs. (57) and (60), the determinants of coefficient matrices $\mathbf{V}^{\mathrm{f}}$ and $\mathbf{R}^{\mathrm{f}}$ in Eqs. (57) and (60) must vanish:

$$|\mathbf{V}^{\mathrm{f}}| = 0, \quad |\mathbf{R}^{\mathrm{f}}| = 0. \tag{63}$$

Because it is difficult to analytically obtain the roots of the transcendental equations with respect to the eigenvalue in Eq. (63), the argument principle and bisection method are applied to obtain the roots [48]. The corresponding unknown constants $\mathbf{C}_{\mathrm{s}}$ and $\mathbf{C}_{\mathrm{a}}$ can then be obtained by substituting the eigenvalues μ_i into Eqs. (57) and (60). Subsequently, all constants can be determined using Eq. (50). Finally, substituting these constants into Eq. (48) yields the corresponding eigenvectors $\boldsymbol{\psi}_i$.

4.3 Eigensolutions for the clamped boundary conditions at $y = \pm h$

Different from the eigensolutions for the free boundary conditions, there is no zero eigenvalue for the clamped

boundary conditions. For the nonzero eigenvalues, because the clamped boundary conditions are symmetric with respect to the x-axis, the general solutions can be categorized into symmetric and antisymmetric deformation solutions, which are given by Eqs. (55) and (56), respectively.

For the symmetric deformation, substituting Eqs. (55) and (50) into Eq. (26) leads to

$$\mathbf{V}^{\mathrm{c}}\mathbf{C}_{\mathrm{s}} = \mathbf{0}, \tag{64}$$

in which the components of the coefficient matrix $\mathbf{V}^{\mathrm{c}}$ are expressed as

$$\begin{aligned} V_{11}^{\mathrm{c}} &= \frac{2G\mu^2(1-\nu_{12}\nu_{21})+E_2\left(\mu^2\nu_{12}-\beta_1^2\right)}{E_1\mu\gamma_2}\cos(\beta_1 h), \\ V_{21}^{\mathrm{c}} &= \frac{2G\left(\nu_{12}\mu^2+\beta_1^2\right)-\nu_{12}\left(\gamma_2+E_2\mu^2\right)}{\beta_1 E_1\gamma_2}\sin(\beta_1 h), \\ V_{31}^{\mathrm{c}} &= -\frac{\gamma_1}{2N^2\mu G\beta_1 E_1\gamma_2}\sin(\beta_1 h). \end{aligned} \tag{65}$$

The expressions for V_{m2}^{c} and V_{m3}^{c} (m = 1, 2, 3) are similar to those for V_{m1}^{c}, with the only difference being the substitution of β_1 with β_2 and β_3, respectively.

For the antisymmetric deformation, substituting Eqs. (56) and (50) into Eq. (26) yields

$$\mathbf{R}^{\mathrm{c}}\mathbf{C}_{\mathrm{a}} = \mathbf{0}, \tag{66}$$

where the components of the coefficient matrix $\mathbf{R}^{\mathrm{c}}$ are expressed as

$$\begin{aligned} R_{11}^{\mathrm{c}} &= \frac{2G\mu^2(1-\nu_{12}\nu_{21})+E_2\left(\mu^2\nu_{12}-\beta_1^2\right)}{\gamma_2 E_1\mu}\sin(\beta_1 h), \\ R_{21}^{\mathrm{c}} &= \frac{\nu_{12}\left(\gamma_2+E_2\mu^2\right)-2G\left(\nu_{12}\mu^2+\beta_1^2\right)}{E_1\beta_1\gamma_2}\cos(\beta_1 h), \\ R_{31}^{\mathrm{c}} &= \frac{\gamma_1}{2N^2\mu G\beta_1 E_1\gamma_2}\cos(\beta_1 h), \end{aligned} \tag{67}$$

and the expressions for R_{m2}^{c} and R_{m3}^{c} (m = 1, 2, 3) are similar to those for R_{m1}^{c}, except that β_1 is replaced with β_2 and β_3, respectively.

Subsequently, the symmetric and antisymmetric eigenvalues for the clamped boundary conditions can be determined by equating the determinants of coefficient matrices $\mathbf{V}^{\mathrm{c}}$ and $\mathbf{R}^{\mathrm{c}}$ in Eqs. (64) and (66) with zero

$$|\mathbf{V}^{\mathrm{c}}| = 0, \quad |\mathbf{R}^{\mathrm{c}}| = 0. \tag{68}$$

Applying the argument principle and bisection method to solve the transcendental equations in Eq. (68) yields the nonzero eigenvalues μ_i, which can be used to determine the corresponding unknown constants $\mathbf{C}_{\mathrm{s}}$ and $\mathbf{C}_{\mathrm{a}}$. Subsequently, by substituting these constants into Eq. (50), all constants can be obtained. Finally, the corresponding eigenvectors $\boldsymbol{\psi}_i$ can be determined using Eq. (48).

4.4 Eigensolutions for the free boundary conditions at $y = h$ and clamped boundary conditions at $y = -h$

Similar to the eigensolutions for the clamped boundary conditions, there is no zero eigenvalue for the boundary conditions in which the edge at $y = h$ is free and the edge at $y = -h$ is clamped. For the nonzero eigenvalues, because the boundary conditions are not symmetric with respect to the x-axis, the general solutions are expressed in Eq. (48). Substituting Eqs. (48) and (50) into Eq. (27) yields

$$\begin{bmatrix} \mathbf{V}^{\mathrm{f}} & \mathbf{R}^{\mathrm{f}} \\ \mathbf{V}^{\mathrm{m}} & \mathbf{R}^{\mathrm{m}} \end{bmatrix} \begin{bmatrix} \mathbf{C}_{\mathrm{s}} \\ \mathbf{C}_{\mathrm{a}} \end{bmatrix} = \mathbf{0}, \tag{69}$$

in which the matrices $\mathbf{V}^{\mathrm{f}}$ and $\mathbf{R}^{\mathrm{f}}$ are given by Eqs. (59) and (62), respectively. The expressions of matrices $\mathbf{V}^{\mathrm{m}}$ and $\mathbf{R}^{\mathrm{m}}$ are similar to those of $\mathbf{V}^{\mathrm{c}}$ and $\mathbf{R}^{\mathrm{c}}$ in Eqs. (65) and (67), except that h is replaced with $-h$. The existence condition of the solution to Eq. (69) is that the determinants of the coefficient matrix vanish, which yields a transcendental equation with respect to the eigenvalues. Applying the argument principle and bisection method to solve the transcendental equation yields the eigenvalues μ_i. Then, by substituting the nonzero eigenvalues into Eq. (69), the corresponding constants $\mathbf{C}_{\mathrm{s}}$ and $\mathbf{C}_{\mathrm{a}}$ are solved. Subsequently, using Eq. (50), all constants can be obtained. Finally, the corresponding eigenvectors $\boldsymbol{\psi}_i$ can be determined based on Eq. (48).

5. Solutions for the orthotropic micropolar plane stress problem

After the eigenvalues and eigenvectors are obtained, according to Eqs. (29) and (31), the solution to Eq. (28) corresponding to the nonzero and zero eigenvalues can be expressed respectively as

$$\mathbf{v}_i = \exp(\mu_i x)\boldsymbol{\psi}_i \quad (\mu_i \neq 0), \tag{70}$$

$$\begin{aligned} &\mathbf{v}_{01}^{(0)} = \boldsymbol{\psi}_{01}^{(0)}, \quad \mathbf{v}_{01}^{(1)} = \boldsymbol{\psi}_{01}^{(1)} + x\boldsymbol{\psi}_{01}^{(0)}, \\ &\mathbf{v}_{02}^{(0)} = \boldsymbol{\psi}_{02}^{(0)}, \quad \mathbf{v}_{02}^{(1)} = \boldsymbol{\psi}_{02}^{(1)} + x\boldsymbol{\psi}_{02}^{(0)}, \\ &\mathbf{v}_{02}^{(2)} = \boldsymbol{\psi}_{02}^{(2)} + x\boldsymbol{\psi}_{02}^{(1)} + \frac{x^2}{2}\boldsymbol{\psi}_{02}^{(0)}, \\ &\mathbf{v}_{02}^{(3)} = \boldsymbol{\psi}_{02}^{(3)} + x\boldsymbol{\psi}_{02}^{(2)} + \frac{x^2}{2}\boldsymbol{\psi}_{02}^{(1)} + \frac{x^3}{6}\boldsymbol{\psi}_{02}^{(0)}. \end{aligned} \tag{71}$$

According to the property of symplectic orthogonality of eigenvectors and expansion theorems [33], the general solution to the orthotropic micropolar plane stress problem can be expressed as follows:

$$\mathbf{v} = \sum_{i=1}^{n} c_i \mathbf{v}_i^* \quad (i = 1, 2, \cdots, n), \tag{72}$$

where n denotes the number of eigenvalues considered, $\mathbf{v}_i^*$ is

one of the solutions in Eqs. (70) and (71), and c_i is an unknown constant to be determined by the boundary conditions at both ends ($x = 0$, L). Subsequently, according to the Hamiltonian variation of Eq. (19) in Sect. 3, the variational equation corresponding to the body force and boundary conditions at both ends can be obtained. Then, substituting Eq. (72) into the variational equation yields a system of linear algebraic equations that provide the unknown constants c_i. The detailed derivation is presented in the following.

The Hamiltonian density function in Eq. (14) is rewritten as

$$H(\mathbf{q},\mathbf{p}) = H^*(\mathbf{q},\mathbf{p}) + \mathbf{q}^{\mathrm{T}}\mathbf{f}, \tag{73}$$

where $\mathbf{f}$ is expressed by Eq. (8). Substituting Eq. (73) into Eq. (19) and implementing the variation, the variational equation corresponding to the body force $\mathbf{f}$ and boundary conditions at both ends can be expressed as

$$\begin{aligned}&\int_{-h}^{h}\left(\delta\mathbf{p}_L^{\mathrm{T}}\right)(\mathbf{q}_L-\bar{\mathbf{q}})\mathrm{d}y+\int_{-h}^{h}\left(\delta\mathbf{q}_0^{\mathrm{T}}\right)(\mathbf{p}_0-\bar{\mathbf{p}})\mathrm{d}y\\&+\int_0^L\int_{-h}^{h}(\delta\mathbf{q}^{\mathrm{T}})\mathbf{f}\mathrm{d}y\mathrm{d}x=0.\end{aligned} \tag{74}$$

The general solution in Eq. (72) can be rewritten as

$$\mathbf{v}=\begin{bmatrix}\mathbf{q}\\ \mathbf{p}\end{bmatrix}=\sum_{i=1}^{n}c_i\begin{bmatrix}\mathbf{q}^i\\ \mathbf{p}^i\end{bmatrix}. \tag{75}$$

Substituting Eq. (75) into Eq. (74) yields

$$\begin{aligned}&\sum_{i=1}^{n}\delta c_i\left\{\sum_{j=1}^{n}c_j\int_{-h}^{h}\left[\left(\mathbf{p}_L^i\right)^{\mathrm{T}}\mathbf{q}_L^j+\left(\mathbf{q}_0^i\right)^{\mathrm{T}}\mathbf{p}_0^j\right]\mathrm{d}y\right.\\&\left.-\int_{-h}^{h}\left[\left(\mathbf{p}_L^i\right)^{\mathrm{T}}\bar{\mathbf{q}}+\left(\mathbf{q}_0^i\right)^{\mathrm{T}}\bar{\mathbf{p}}\right]\mathrm{d}y+\int_0^L\int_{-h}^{h}(\mathbf{q}^i)^{\mathrm{T}}\mathbf{f}\mathrm{d}y\mathrm{d}x\right\}=0.\end{aligned} \tag{76}$$

Because $\delta c_i\,(i = 1,\ 2,\ \cdots,\ n)$ is arbitrary, a set of algebraic equations for solving the unknown constants can be established as

$$\begin{bmatrix}a_{11}&a_{12}&\cdots&a_{1n}\\ a_{21}&a_{22}&\cdots&a_{2n}\\ \vdots&\vdots&&\vdots\\ a_{n1}&a_{n2}&\cdots&a_{nn}\end{bmatrix}\begin{bmatrix}c_1\\ c_2\\ \vdots\\ c_n\end{bmatrix}=\begin{bmatrix}d_1\\ d_2\\ \vdots\\ d_n\end{bmatrix}, \tag{77}$$

where

$$\begin{aligned}&a_{ij}=\int_{-h}^{h}\left[\left(\mathbf{p}_L^i\right)^{\mathrm{T}}\mathbf{q}_L^j+\left(\mathbf{q}_0^i\right)^{\mathrm{T}}\mathbf{p}_0^j\right]\mathrm{d}y,\\&(i,j=1,\ 2,\ \cdots,\ n),\\&d_i=\int_{-h}^{h}\left[\left(\mathbf{p}_L^i\right)^{\mathrm{T}}\bar{\mathbf{q}}+\left(\mathbf{q}_0^i\right)^{\mathrm{T}}\bar{\mathbf{p}}\right]\mathrm{d}y-\int_0^L\int_{-h}^{h}(\mathbf{q}^i)^{\mathrm{T}}\mathbf{f}\mathrm{d}y\mathrm{d}x,\\&(i=1,\ 2,\ \cdots,\ n).\end{aligned} \tag{78}$$

The unknown constants c_i can be determined by solving Eq. (77); then, the solution to the original problem is obtained.

6. Numerical examples

In this section, three examples are presented to illustrate the accuracy and validity of the proposed method. In Sect. 6.1, the results of the proposed approach are compared with those obtained from FEM to validate its convergence and accuracy. In Sect. 6.2, the relationships between the size-dependent behaviour and material parameters of the orthotropic micropolar plane stress problem are investigated using the proposed approach. In Sect. 6.3, the mechanical behaviour of the lattice structures is analyzed using the proposed method, and the results are compared with those of FEM.

6.1 Convergence and accuracy analysis

In this subsection, an orthotropic micropolar plane stress problem with three types of homogeneous boundary conditions at the edges $y = \pm h$ is first presented as follows: (1) the two edges at $y = \pm h$ are free, the edge at $x = 0$ is clamped, and a shear traction F is applied along edge $x = L$, as shown in Fig. 2(a); (2) the edges at $y = \pm h$ are fixed, the edge at $x = 0$ is free, and a uniformly distributed pressure F is applied along the edge at $x = L$, as depicted in Fig. 2(b); and (3) the edge at $y = -h$ is fixed, the edges at $y = h$ and $x = 0$ are free, and a uniformly distributed pressure F is applied along the edge at $x = L$, as displayed in Fig. 2(c). The length and width of the microplate are 3 mm and 2 mm, respectively. In addition, the values of the material parameters and the load F are listed in Table 1.

According to the properties of the Hamiltonian eigenvalue problem, six different complex domains are used to calculate the eigenvalues of the proposed approach for three types of homogeneous boundary conditions: $\mathrm{Re}(\mu) \in (0, 40]$, $(0, 80]$, $(0, 140]$, $(0, 190]$, $(0, 230]$, $(0, 250]$, and $\mathrm{Im}(\mu) \in (0, 20]$. The results at point $(1.5, -0.5)$ obtained from the proposed approach corresponding to the six different complex domains of the eigenvalues are compared with the convergent results computed using FEM with 1500 × 1500 elements, as listed in Tables 2-4. Evidently, an increasing number of eigenvalues leads to gradually converging results, and the convergent results align with those obtained by FEM for the first three or four significant digits. These results indicate the accuracy of the proposed approach in solving the micropolar plane stress problem with three types of homogeneous boundary conditions.

The results obtained from the micropolar elasticity theory should be reduced to those from the classical elasticity theory when the parameters N, l_x, and l_y are small [49]. Therefore, to further verify the accuracy of the proposed approach, its results using the parameters $N = 0.003$,

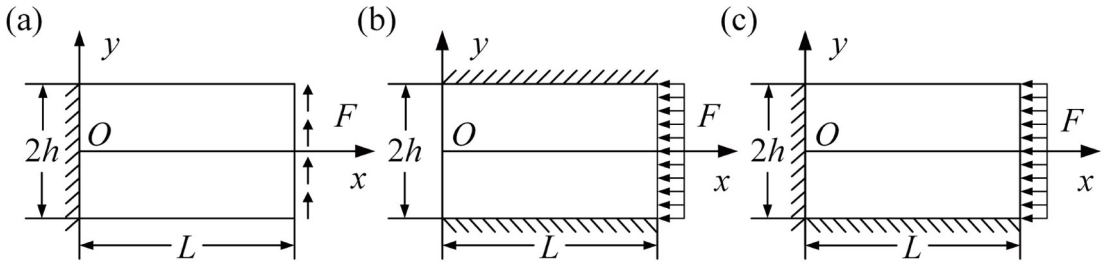

Figure 2 Micropolar plane stress problem with three types of homogeneous boundary conditions at edges $y = \pm h$.

Table 1 Material parameters and load of the problem with homogeneous boundary conditions in Example 1

E_1 (Mpa)	E_2 (Mpa)	ν_{12}	ν_{21}	G (Mpa)	N	l_x (mm)	l_y (mm)	F (Mpa)
150	100	0.375	0.25	40	0.5	0.25	0.4	0.05

Table 2 Results of the proposed approach for the case (1) at point $(1.5, -0.5)$

	Present method with different numbers of eigenvalue						FEM mesh 1500 × 1500
	76	152	262	356	432	466	
u (nm)	1278.296	1278.150	1278.111	1278.100	1278.094	1278.093	1278.083
v (nm)	3982.440	3981.928	3981.786	3981.736	3981.723	3981.722	3981.678
θ (nrad)	3231.535	3231.257	3231.184	3231.163	3231.152	3231.150	3231.129
σ_{xx} (kPa)	92.464	92.464	92.465	92.465	92.465	92.465	92.465
τ_{xy} (kPa)	53.161	53.161	53.161	53.162	53.162	53.162	53.159
m_{xz} (kPa)	12.943	12.943	12.944	12.944	12.944	12.944	12.944

Table 3 Results of the proposed approach for the case (2) at point $(1.5, -0.5)$

	Present method with different numbers of eigenvalue						FEM mesh 1500 × 1500
	70	146	256	350	426	462	
u (nm)	93.217	93.256	93.266	93.269	93.270	93.270	93.272
v (nm)	8.516	8.517	8.518	8.518	8.518	8.518	8.518
θ (nrad)	−14.437	−14.443	−14.445	−14.445	−14.446	−14.446	−14.446
σ_{xx} (kPa)	11.798	11.803	11.804	11.804	11.804	11.804	11.807
τ_{xy} (kPa)	4.655	4.656	4.656	4.656	4.656	4.656	4.659
m_{xz} (kPa)	−0.114	−0.114	−0.114	−0.114	−0.114	−0.114	−0.114

Table 4 Results of the proposed approach for the case (3) at point $(1.5, -0.5)$

	Present method with different numbers of eigenvalue						FEM mesh 1500 × 1500
	150	296	522	706	854	928	
u (nm)	284.426	284.489	284.509	284.514	284.516	284.516	284.519
v (nm)	0.218	0.207	0.202	0.201	0.201	0.201	0.202
θ (nrad)	−173.718	−173.752	−173.763	−173.766	−173.767	−173.767	−173.768
σ_{xx} (kPa)	12.108	12.111	12.113	12.113	12.113	12.113	12.122
τ_{xy} (kPa)	17.496	17.497	17.498	17.498	17.499	17.499	17.502
m_{xz} (kPa)	−0.331	−0.331	−0.332	−0.332	−0.332	−0.332	−0.333

$l_x = 0.0025$ mm and $l_y = 0.005$ mm are compared with those of ANSYS based on the classical elastic theory for the three types of homogeneous boundary conditions. Because the classical elasticity theory cannot consider microrotation, the displacements u, v and stresses σ_{xx}, τ_{xy} at point $(1.5, 0.5)$ are presented in Table 5. It can be seen that when the values of parameters N, l_x, and l_y are all small, the results obtained from the proposed approach are consistent with those of the classical elasticity theory for the first three to four significant digits, indicating the accuracy of the proposed approach.

The aforedescribed analysis concerns the solutions of the orthotropic micropolar plane stress problem with homogeneous boundary conditions at edges $y = \pm h$. For common nonhomogeneous boundary conditions on the two opposite edges, analytical solutions can also be obtained using the proposed method and superposition principle, which is described as follows. Consider an orthotropic microplate with distributed loads $F_1 = 2F\sin(x\pi/L)$ and $F_2 = 2F\cos(y\pi/2h)$ applied along edges $y = -h$ and $x = L$, respectively. The edge at $y = h$ is free, and that at $x = 0$ is clamped. The parameters N, l_x, and l_y are 0.6, 0.25 mm, and 0.3 mm, respectively, whereas the other material parameters and geometric size are the same as those described above for the microplate with homogeneous boundary conditions at edges $y = \pm h$. According to the superposition principle, this problem can be divided into two subproblems with homogeneous boundary conditions at edges $y = \pm h$: (1) the two opposite edges $y = \pm h$ are free, the edge $x = 0$ is clamped, and the load F_2 is imposed along edge $x = L$; and (2) the edges $y = h$ and $x = L$ are free, the edge $x = 0$ is fixed, and the load F_1 is imposed along edge $y = -h$.

The results at points $(1.5, -0.5)$, $(1.5, 0)$, and $(1.5, 0.5)$ calculated from the proposed approach and FEM are presented in Table 6. To ensure convergence, the complex domain of the eigenvalues is taken as $\mathrm{Re}(\mu) \in (0, 200]$ and $\mathrm{Im}(\mu) \in (0, 20]$, and 1500×1500 elements are used in FEM. Table 6 indicates that the results obtained from the proposed approach align with those obtained from FEM for the first three or four significant digits, which also shows that the proposed method can be used for solving some problems with non-homogeneous boundary conditions by superimposing some of the three types of homogeneous boundary conditions. In addition, the nephograms of the displacements and stresses are shown in Fig. 3.

6.2 Analysis of the size-dependent behaviour of the orthotropic micropolar plane stress problem

In this subsection, to analyze the size-dependent behaviour of the orthotropic micropolar plane stress problem, the dimensionless parameters are first defined as

$$\bar{l}_x = \frac{l_x}{L}, \quad \bar{l}_y = \frac{l_y}{2h}. \tag{79}$$

Consider a micropolar planar plate with various values of nondimensional coupling factors and nondimensional material characteristic lengths. The other material parameters, geometric size, and boundary conditions are the same as those of case (1) in Sect. 6.1.

For comparison, we consider a classical planar plate with the same Young's modulus, Poisson's ratio, shear modulus, geometric size, and boundary conditions as those of the micropolar model. According to Hassanpour's conclusion [50], when simplifying the micropolar elasticity theory to the classical elasticity theory, the displacements u, v and stresses σ_{xx}, τ_{xy} obtained from the micropolar elasticity theory are equal to those from the classical elasticity theory, and the microrotation θ and couple stress m_{xz} can be expressed as

$$\theta = \frac{1}{2}\left(\frac{\partial v}{\partial x} - \frac{\partial u}{\partial y}\right), \quad m_{xz} = 0. \tag{80}$$

We first investigate the distributions of displacements and stresses along line $y = -h/2$ with $\bar{l}_x = \bar{l}_y = 1$, 0.5, 0.25, 0.1, 0.05, and 0.005 when the value of N is 0.4, as shown in Fig. 4. Evidently, the differences between the results ob-

Table 5 Results of the proposed approach and ANSYS at point $(1.5, 0.5)$ for three cases of homogeneous boundary conditions

	Case (1)		Case (2)		Case (3)	
	Present	ANSYS	Present	ANSYS	Present	ANSYS
u (μm)	1.5638	1.5638	0.1398	0.1398	1.1667	1.1662
v (μm)	4.9207	4.9206	0.0118	0.0118	−0.0523	−0.0523
σ_{xx} (kPa)	111.8172	111.8157	14.3803	14.3858	25.0878	25.0860
τ_{xy} (kPa)	56.0847	56.0847	8.8855	8.8817	13.8692	13.8610

Table 6 Results of the proposed approach and FEM at points $(1.5, -0.5)$, $(1.5, 0)$ and $(1.5, 0.5)$ for micropolar plane stress problem with the non-homogeneous boundary conditions

	$(1.5, -0.5)$		$(1.5, 0)$		$(1.5, 0.5)$	
	Present	FEM	Present	FEM	Present	FEM
u (μm)	−0.38844	−0.38835	0.53054	0.53053	1.42964	1.42912
v (μm)	−4.41441	−4.41430	−4.19141	−4.19225	−4.16394	−4.16384
θ (μrad)	−2.50260	−2.50286	−2.43643	−2.43628	−2.48369	−2.48374
σ_{xx} (kPa)	18.41031	18.41017	62.77483	62.77615	106.52050	106.52469
τ_{xy} (kPa)	−48.56614	−48.56461	−58.75368	−58.75534	−51.67939	−51.67707
m_{xz} (kPa)	−0.87819	−0.87869	−2.20023	−2.20077	−2.20390	−2.20347

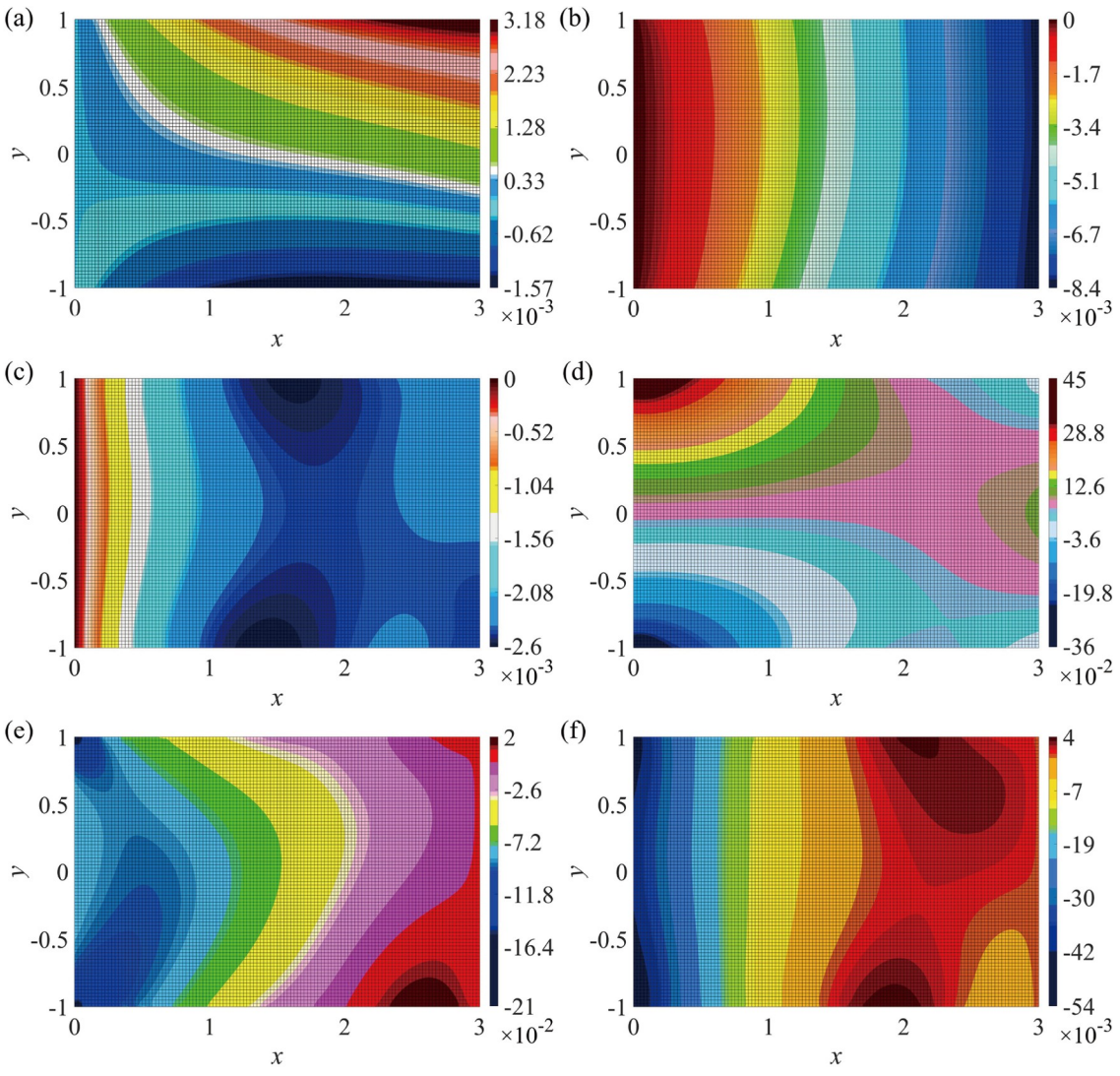

Figure 3 Nephograms of the displacements and stresses for the orthotropic micropolar plane stress problem with nonhomogeneous boundary conditions. (a) The displacement u (mm); (b) the displacement v (mm); (c) the microrotation θ (mrad); (d) the normal stress σ_{xx} (MPa); (e) the shear stress τ_{xy} (MPa); (f) the couple stress m_{xz} (MPa).

tained by the micropolar theory and those by the classical elasticity theory gradually increase with an increase in $\bar{l}_x$ and $\bar{l}_y$. This indicates that the size effect is more significant when the coupling factor and characteristic lengths are large.

We then investigate the distributions of displacements and stresses along line $y = -h/2$ with $\bar{l}_x = \bar{l}_y = 1$, 0.5, 0.25, 0.1, 0.05, and 0.005 when the value of N is 0.05, as depicted in Fig. 5. Figure 5(a)-(d) indicate that the results obtained from the micropolar elasticity theory are close to those from the classical elasticity theory, regardless of the characteristic lengths. However, Fig. 5(e) and (f) show that the differences between the results obtained by the micropolar theory and those by Eq. (80) gradually increase with increasing $\bar{l}_x$ and $\bar{l}_y$. This implies that when the coupling factor is small, no size effect occurs for the displacements u, v and stresses σ_{xx}, τ_{xy}, but the microrotation θ and couple stress m_{xz} are still affected by the size effect.

Subsequently, we investigate the distributions of displacements and stresses along line $y = -h/2$ with $N = 0.9$, 0.6, 0.4, 0.2, 0.1, and 0.05 when $\bar{l}_x$ and $\bar{l}_y$ are both 0.5, as displayed in Fig. 6. It can be seen from Fig. 6 that the displacements u, v and stresses σ_{xx}, τ_{xy}, and m_{xz} are gradually away from the results by the classical elasticity with increasing coupling factor N, whereas the microrotation θ is gradually away from the results by the classical elasticity with decreasing coupling factor N. These results indicate that when the characteristic lengths are large, for displacements u, v and stresses σ_{xx}, τ_{xy}, and m_{xz}, the size effect is more significant when the coupling factor increases. However, for the microrotation θ, the size effect is more significant when the coupling factor decreases.

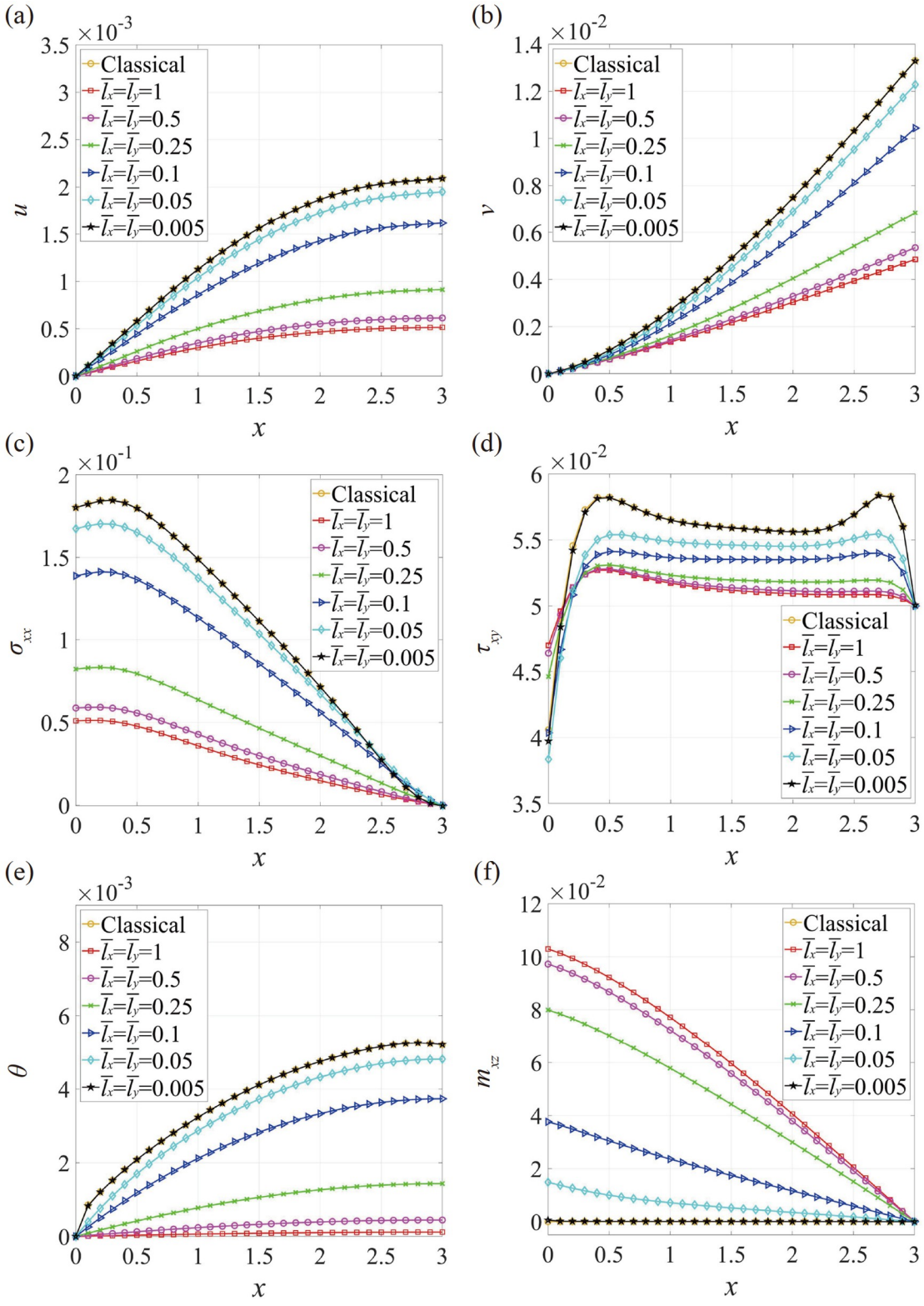

Figure 4 Variations of displacements and stresses with different $\bar{l}_x$ and $\bar{l}_y$ along line $y=-h/2$ when N is 0.4.

Next, we investigate the distributions of displacements and stresses along line $y=-h/2$ with $N=0.9$, 0.6, 0.4, 0.2, 0.1, and 0.05 when both $\bar{l}_x$ and $\bar{l}_y$ are 0.0005, as shown in Fig. 7. Figure 7(a)-(e) indicate that the distributions of displacements u, v, stresses σ_{xx}, τ_{xy}, and microrotation θ are close to those from the classical elasticity theory, regardless of the value of the coupling factor N. Based on Fig. 7(f), the values of the couple stress m_{xz} corresponding to different

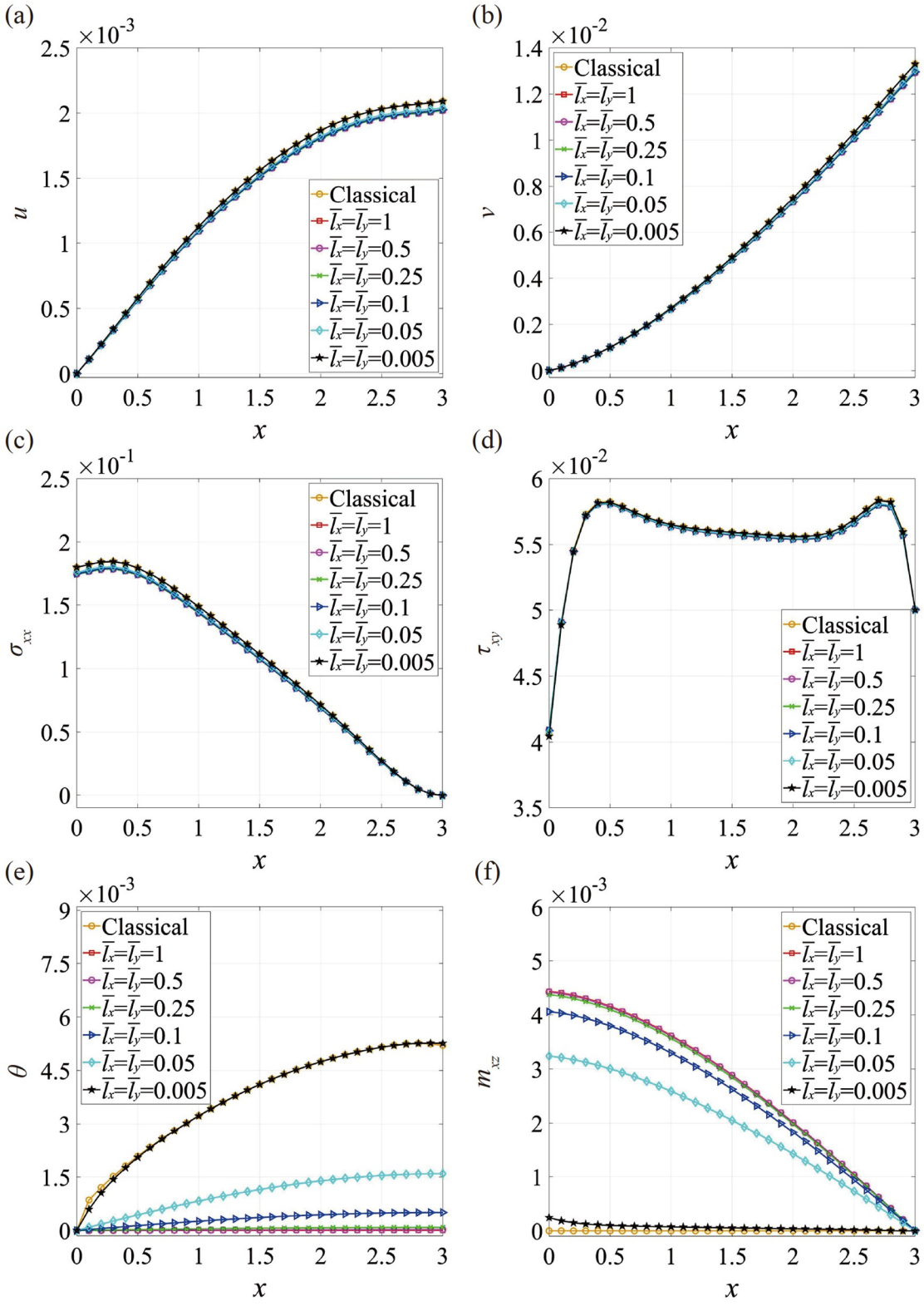

Figure 5 Variations of displacements and stresses with different $\bar{l}_x$ and $\bar{l}_y$ along line $y=-h/2$ when N is 0.05.

values of N are all very small. This implies that when the characteristic lengths are small, the size effect can be ignored.

Because the characteristic lengths $\bar{l}_x$ and $\bar{l}_y$ are independent of each other for the orthotropic micropolar plane stress problem, we investigate the distributions of displacements and stresses along line $y=-h/2$ with $\bar{l}_x=1$, 0.5, 0.25, 0.1, 0.05, and 0.005 when N is 0.4 and $\bar{l}_y$ is 0.5, as depicted in Fig. 8. It can be seen from Fig. 8 that the dif-

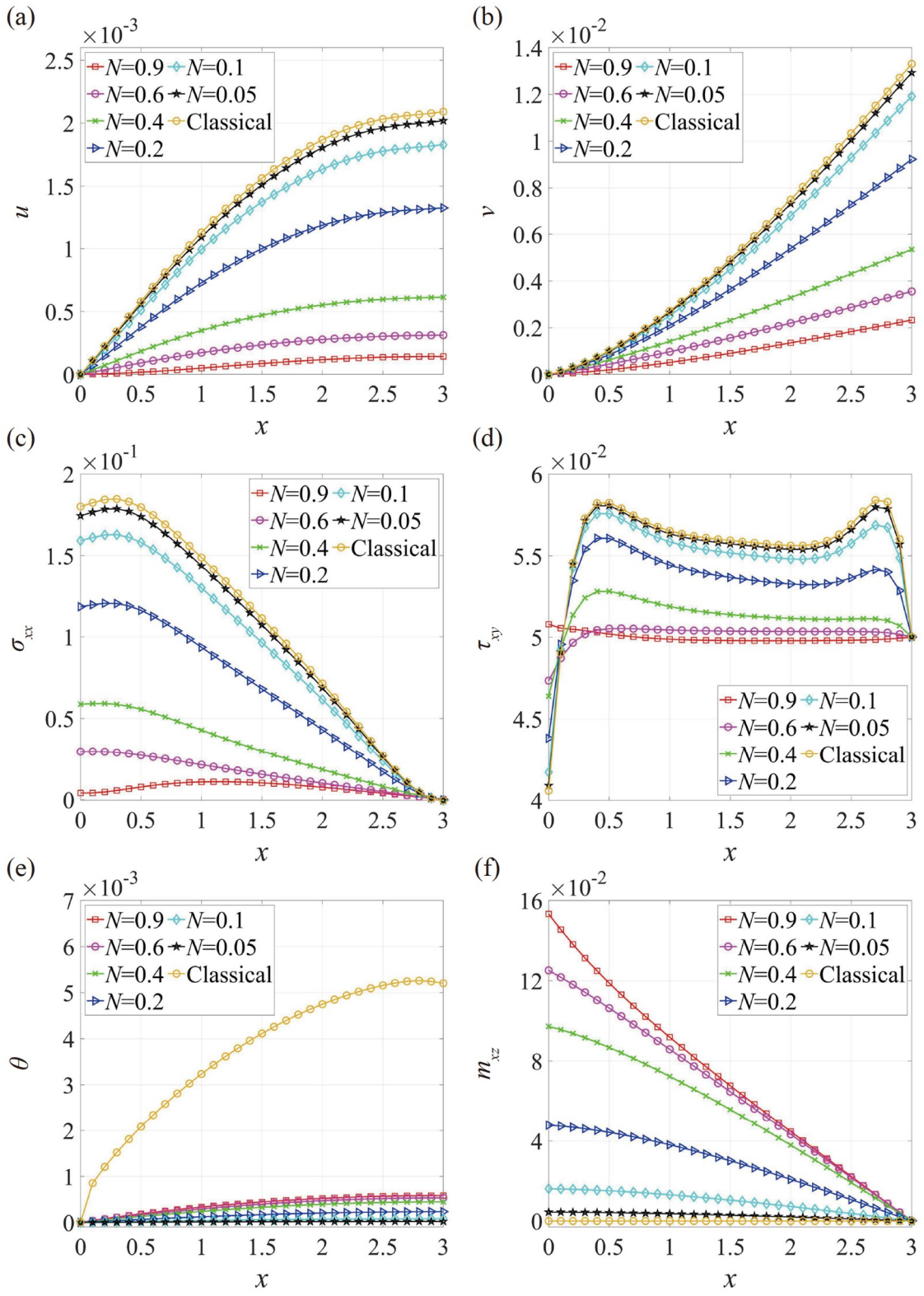

Figure 6 Variations of displacements and stresses with different N along line $y=-h/2$ when $\bar{l}_x$ and $\bar{l}_y$ are both 0.5.

ferences between the results obtained from the micropolar theory and those from the classical elasticity theory gradually decrease with the reduction in $\bar{l}_x$. However, in contrast to the results with $\bar{l}_x = \bar{l}_y = 0.005$ in Fig. 4, when $\bar{l}_x$ is 0.005, there are still differences between the results obtained by the micropolar theory and those by the classical elasticity theory. This suggests that the size effect cannot be ignored when one of the characteristic lengths is small but the other is large.

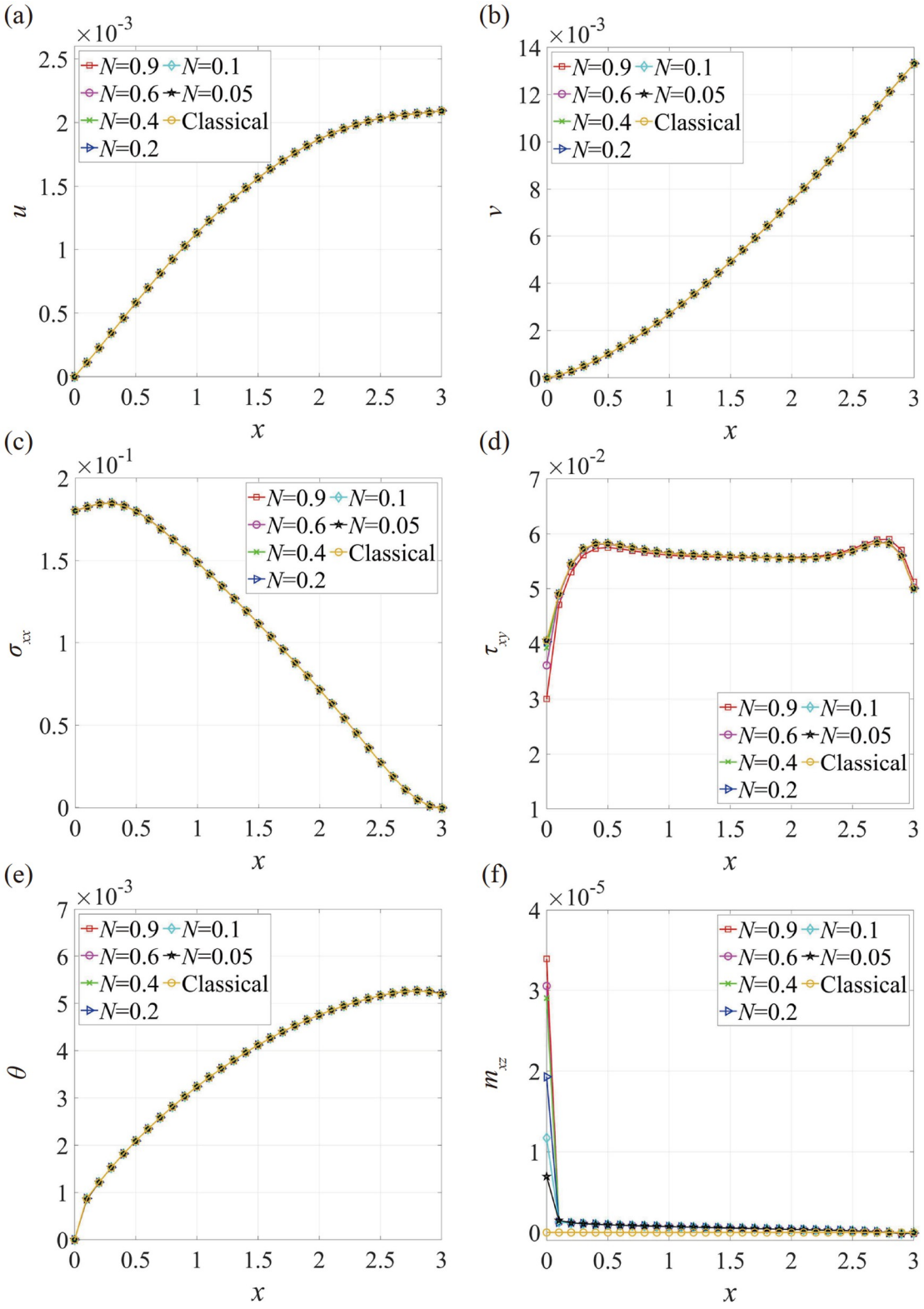

Figure 7 Variations of displacements and stresses with different N along line $y=-h/2$ when $\bar{l}_x$ and $\bar{l}_y$ are both 0.0005.

6.3 Analysis of lattice structures based on the proposed method

Lattice structures composed of periodic cellular topologies are commonly used in weight-critical applications as novel ultralight multifunctional materials [24]. One of the main methods of analyzing their mechanical behaviour is the equivalent continuum approximation, which homogenizes the lattice structures to the micropolar continuum by treating the lattice using beam mechanics [14,51]. The mechanical

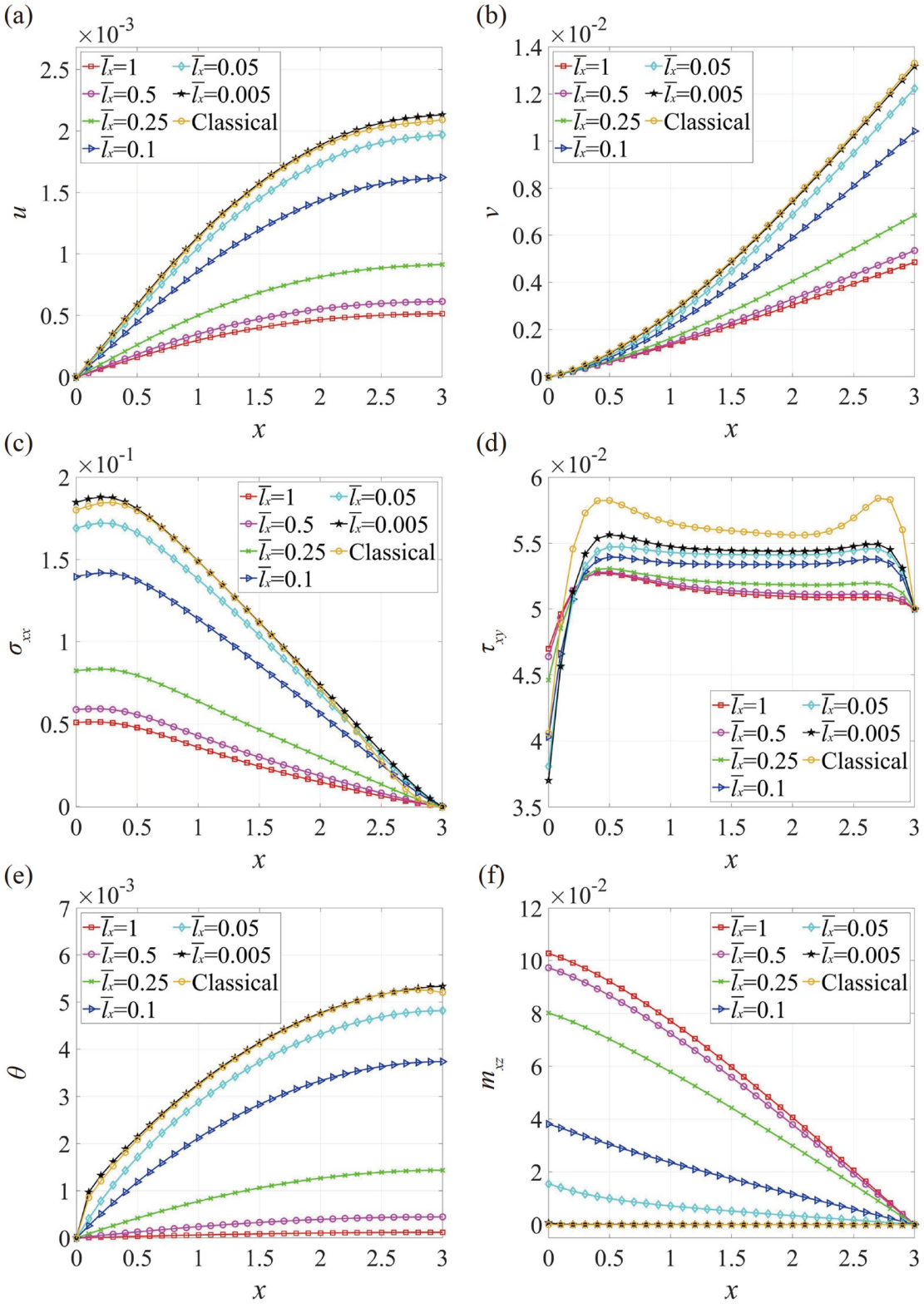

Figure 8 Variations of displacements and stresses with different $\bar{l}_x$ along line $y=-h/2$ when N is 0.4 and $\bar{l}_y$ is 0.5.

behaviour can then be analyzed by an analytical method or FEM based on the micropolar theory. In this subsection, the mechanical behaviour of lattice structures is analyzed using the proposed method.

We consider three rectangular blocks composed of mixed triangle A, mixed triangle B, and hexagonal lattice topologies, as illustrated in Fig. 9. There are 128 and 64 cells along the x and y directions, respectively. The characteristic length

L and thickness h for the three lattice topologies are all taken as 0.2 mm and 0.02 mm, respectively, and the cell wall material is assumed to be isotropic linear elastic with a Young's modulus E of 210 GPa and Poisson's ratio ν of 0.3. The bottoms of these blocks are fixed while both side boundary surfaces are free, and there are three types of boundary conditions on the top surfaces: (1) a concentrated force $F_1 = 10$ MPa is applied at the centre point of the top surface of the rectangular block composed of mixed triangular cell structure A, as displayed in Fig. 9(a); (2) a uniformly distributed shear force $F_2 = 1$ MPa is applied on the top surface of the rectangular block composed of mixed triangular cell structure B, as illustrated in Fig. 9(b); and (3) a uniformly distributed pressure $F_3 = 1$ MPa is applied on the top surface of the rectangular block composed of hexagonal cell structure, as shown in Fig. 9(c). The constitutive relations of these three lattice topologies under the equivalent continuum approximation can be written as [27,52]

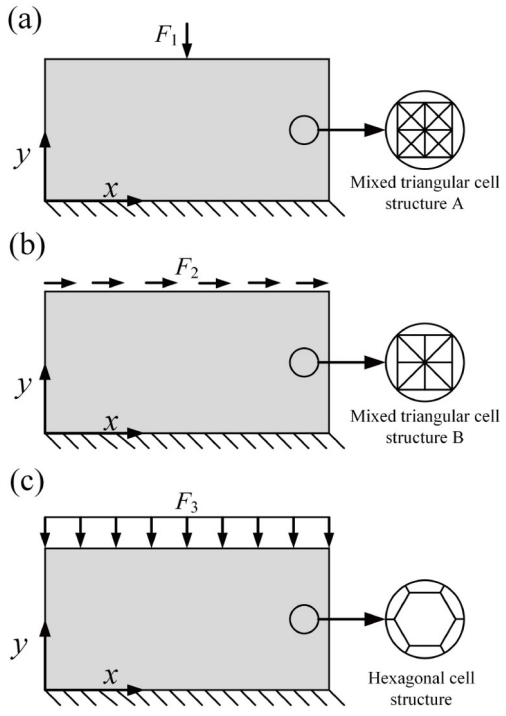

Figure 9 Structures made of lattice topologies with three types of boundary conditions.

$$\boldsymbol{\sigma} = \mathbf{D}\boldsymbol{\varepsilon}, \tag{81}$$

in which

$$\begin{aligned} \boldsymbol{\sigma} &= \left[\sigma_{xx} \quad \sigma_{yy} \quad \tau_{xy} \quad \tau_{yx} \quad m_{xz} \quad m_{yz}\right]^{\mathrm{T}}, \\ \boldsymbol{\varepsilon} &= \left[\varepsilon_{xx} \quad \varepsilon_{yy} \quad \gamma_{xy} \quad \gamma_{yx} \quad \chi_{xz} \quad \chi_{yz}\right]^{\mathrm{T}}, \end{aligned} \tag{82}$$

and the non-zero components of the matrix **D** are listed in Table 7.

For comparison, the lattice structures are also analyzed by a detailed discrete computation based on FEM, in which the cell walls are modelled using beam elements. The nephograms of displacements u and v of the current method and discrete simulation are plotted in Figs. 10-12 for the mixed triangle A, mixed triangle B, and hexagonal lattice topologies, respectively. Figures 10-12 indicate that the results using the proposed approach agree well with those of the detailed discrete computation. To further verify the accuracy of the proposed approach for analyzing lattice structures, we calculate the errors of displacements u and v on lattice nodes between the proposed method and detailed discrete computation within a specified region $x \in [20L, 105L]$ and $y \in [14L, 50L]$ for the three types of lattice structures. As depicted in Fig. 13, the maximum errors of displacements u and v for the three types of lattice structures are all less than 3.1%. Therefore, the proposed approach can be applied to

Table 7 Micropolar elastic constants for three lattice topologies under the equivalent continuum approximation

	Mixed triangle A	Mixed triangle B	Hexagonal
D_{11}	$\frac{Eh}{L^3}\left[\left(1+\frac{\sqrt{2}}{2}\right)L^2+h^2\right]$	$\frac{Eh}{4L^3}[(4+\sqrt{2})L^2+h^2]$	$\frac{Eh\sqrt{3}(L^2+3h^2)}{6L(L^2+h^2)}$
D_{22}	$\frac{Eh}{L^3}\left[\left(1+\frac{\sqrt{2}}{2}\right)L^2+h^2\right]$	$\frac{Eh}{4L^3}[(4+\sqrt{2})L^2+h^2]$	$\frac{Eh\sqrt{3}(L^2+3h^2)}{6L(L^2+h^2)}$
D_{12}	$\frac{Eh}{L^3}\left(\frac{\sqrt{2}}{2}L^2-h^2\right)$	$\frac{-Eh}{4L^3}(h^2-\sqrt{2}L^2)$	$\frac{Eh\sqrt{3}(L^2-h^2)}{6L(L^2+h^2)}$
D_{33}	$\frac{Eh}{L^3}\left(\frac{\sqrt{2}}{2}L^2+2h^2\right)$	$\frac{Eh}{4L^3}(\sqrt{2}L^2+5h^2)$	$\frac{Eh^3\sqrt{3}(9L^2+h^2)}{24L^3(L^2+h^2)}$
D_{44}	$\frac{Eh}{L^3}\left(\frac{\sqrt{2}}{2}L^2+2h^2\right)$	$\frac{Eh}{4L^3}(\sqrt{2}L^2+5h^2)$	$\frac{Eh^3\sqrt{3}(9L^2+h^2)}{24L^3(L^2+h^2)}$
D_{34}	$\frac{Eh}{L^3}\left(\frac{\sqrt{2}}{2}L^2-h^2\right)$	$\frac{-Eh}{4L^3}(h^2-\sqrt{2}L^2)$	$\frac{Eh^3\sqrt{3}(7L^2-h^2)}{24L^3(L^2+h^2)}$
D_{55}	$\frac{2Eh^3}{3L}$	$\frac{2Eh^3}{3L}$	$\frac{7Eh^3\sqrt{3}}{144L}$
D_{66}	$\frac{2Eh^3}{3L}$	$\frac{2Eh^3}{3L}$	$\frac{7Eh^3\sqrt{3}}{144L}$

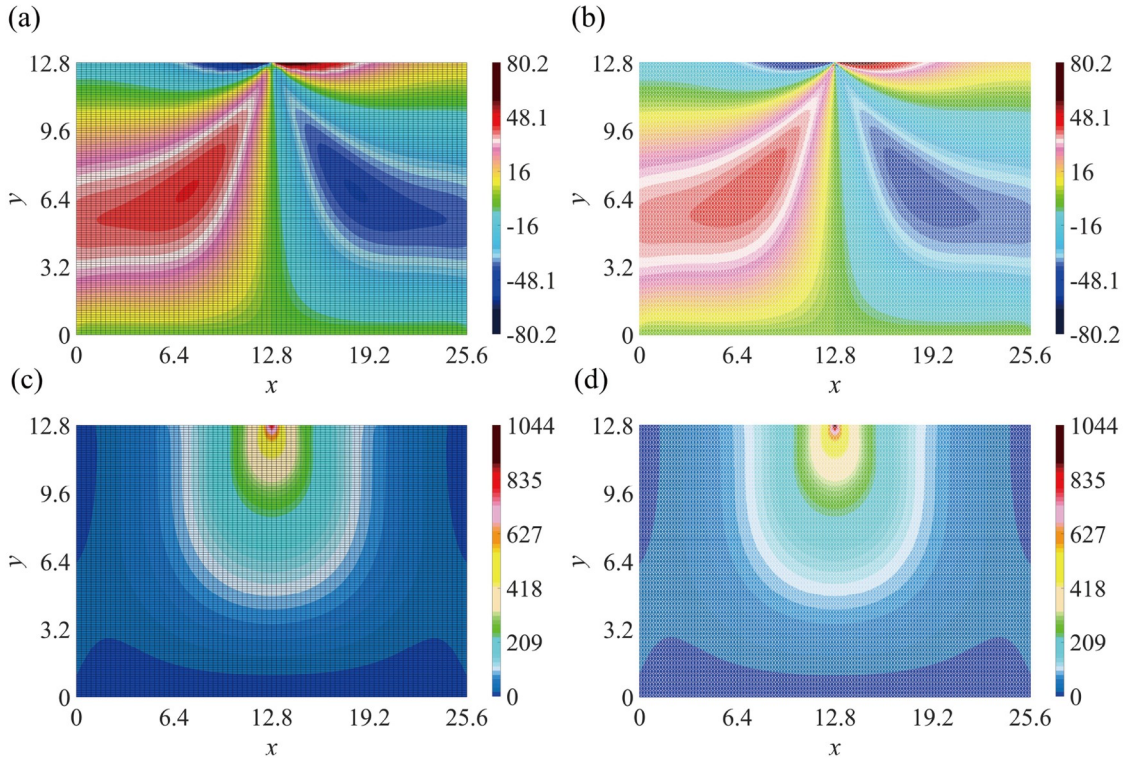

Figure 10 Nephograms of displacements u and v of a structure composed of mixed triangular cell structure A with the concentrated force F_1 applied on the top surface. (a) The displacement u (mm) computed by the proposed method; (b) the displacement u (mm) computed by ANSYS; (c) the displacement v (mm) computed by the proposed method; (d) the displacement v (mm) computed by ANSYS.

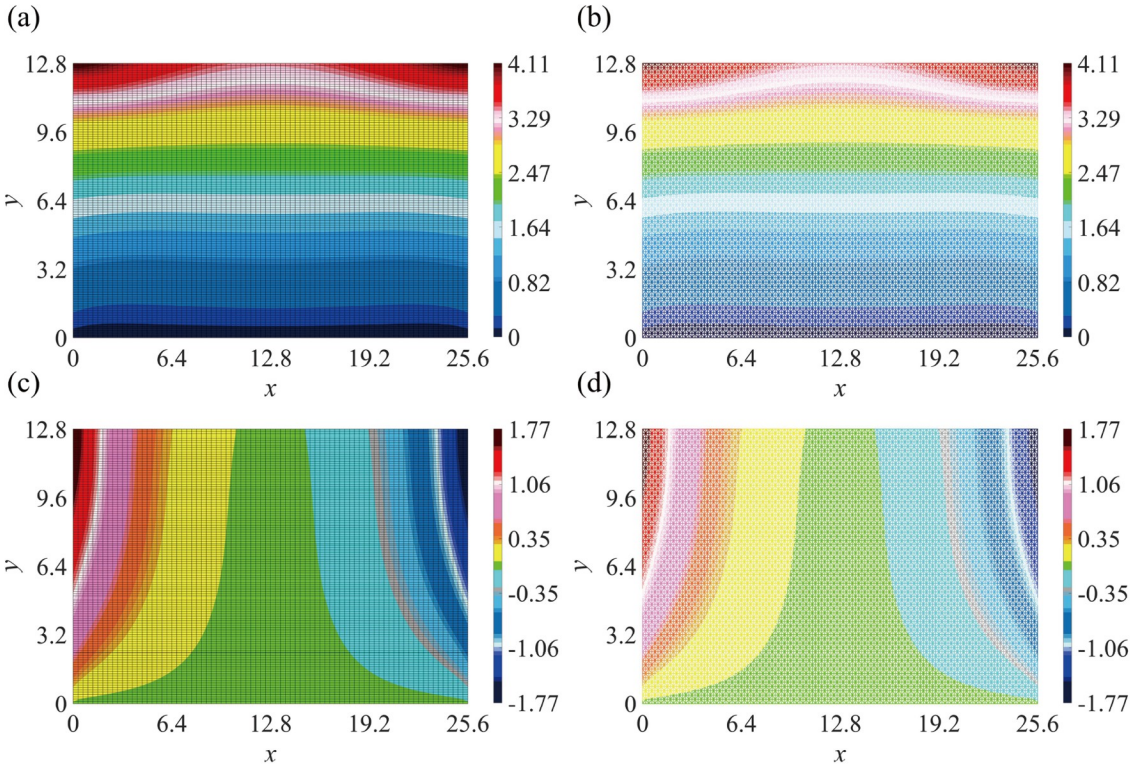

Figure 11 Nephograms of displacements u and v of a structure composed of mixed triangular cell structure B with the shear force F_2 applied on the top surface. (a) The displacement u (mm) computed by the proposed method; (b) the displacement u (mm) computed by ANSYS; (c) the displacement v (mm) computed by the proposed method; (d) the displacement v (mm) computed by ANSYS.

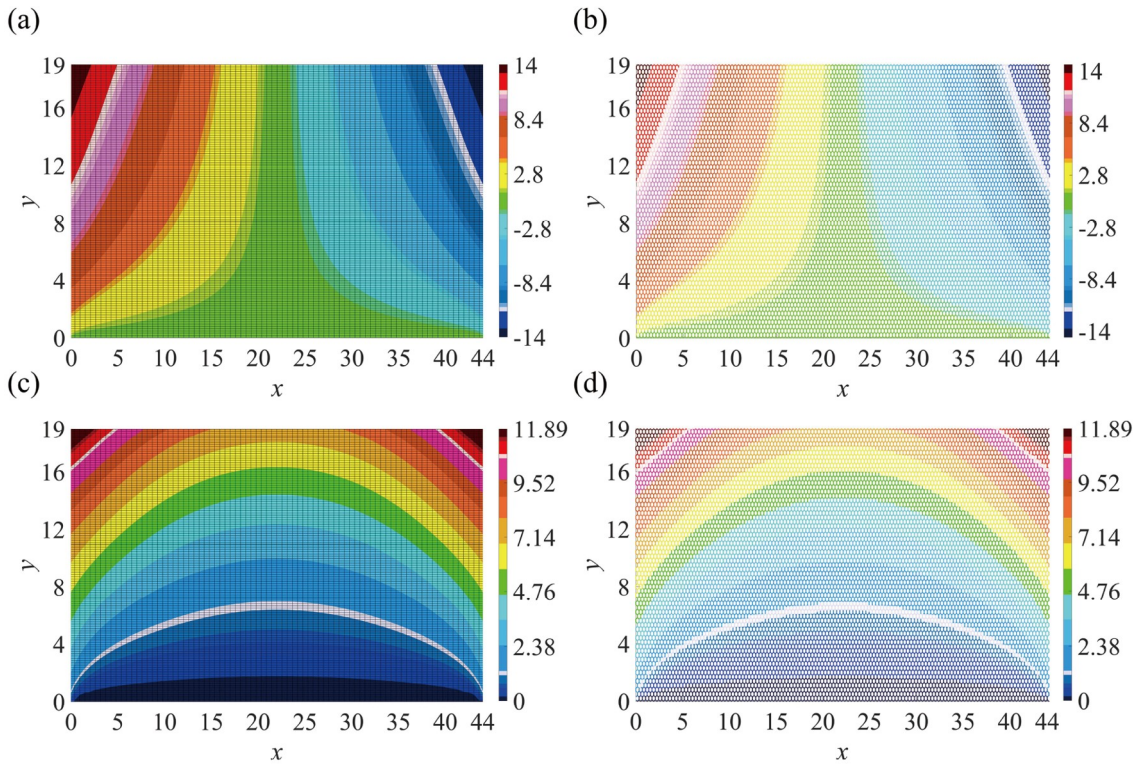

Figure 12 Nephograms of displacements u and v of a structure composed of hexagonal cell structure with the uniformly distributed pressure F_3 applied on the top surface. (a) The displacement u (mm) computed by the proposed method; (b) the displacement u (mm) computed by ANSYS; (c) the displacement v (mm) computed by the proposed method; (d) the displacement v (mm) computed by ANSYS.

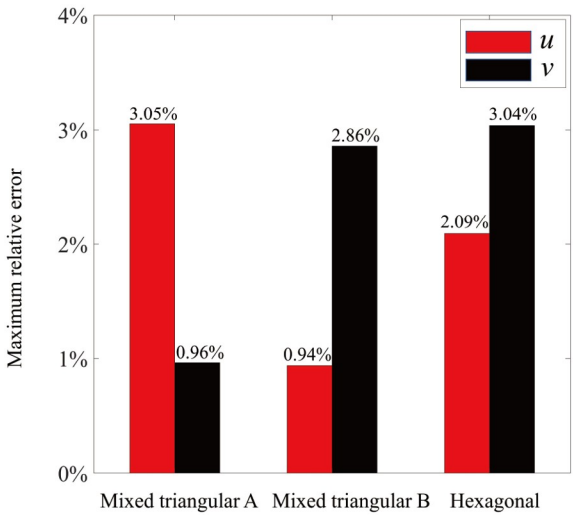

Figure 13 Maximum relative errors of displacements u and v on lattice nodes between the proposed method and the discrete analyses for three types of lattice topologies.

the analysis of lattice structures using an equivalent micropolar continuum approximation.

7. Conclusions

The main objective of this study is to present analytical solutions for the orthotropic microplate plane stress problem using a symplectic approach. By applying Legendre's transformation and the Hamiltonian mixed energy variational principle, the Hamiltonian canonical equation for the orthotropic microplate plane stress problem was obtained. Subsequently, using the method of separation of variables, the homogeneous Hamiltonian canonical equation was transformed into an eigenproblem of the Hamiltonian operator matrix. We derived the eigensolutions of the eigenproblem for three types of homogeneous boundary conditions. Based on the adjoint symplectic orthogonality of the eigensolutions and expansion theorems, the solutions to the orthotropic micropolar plane stress problem were expressed as a series expansion of the eigensolutions.

The numerical results verified the validity of the symplectic method for the orthotropic micropolar plane stress problem under various boundary conditions and showed the relationships between the size effect and material parameters. The results indicate that the micropolar elasticity theory can be simplified into the classical elasticity theory for small characteristic lengths; when the characteristic lengths and coupling factor are all large, the size effect is significant; when the characteristic lengths are large and the coupling factor is small, no size effect occurs for the displacements and force stresses, but the microrotation and couple stress are still affected by the size effect. Further-

more, the proposed approach was applied to analyze lattice structures under an equivalent micropolar continuum approximation.

Conflict of interest *On behalf of all authors, the corresponding author states that there is no conflict of interest.*

Author contributions ***Long Chen****: Methodology, Software, Visualization, Writing – original draft, Writing – review & editing.* ***Zhaofei Tang****: Methodology, Writing – review & editing.* ***Qiong Wu****: Methodology, Software.* ***Qiang Gao****: Conceptualization, Methodology, Writing – review & editing.*

Acknowledgements *This work was supported by the National Key R&D Program of China (Grant No. 2022YFB4201200), Technology Major Project (Grant No. J2019-IV-0019-0087), and National Science and Technology Major Project (Grant No. J2019-IV-0019-0087).*

1 M. Arefi, and A. M. Zenkour, Nonlocal electro-thermo-mechanical analysis of a sandwich nanoplate containing a Kelvin-Voigt viscoelastic nanoplate and two piezoelectric layers, Acta Mech. **228**, 475 (2017).
2 C. L. Cheng, H. C. Chang, C. I. Chang, and W. Fang, Development of a CMOS MEMS pressure sensor with a mechanical force-displacement transduction structure, J. Micromech. Microeng. **25**, 125024 (2015).
3 A. Vergara, T. Tsukamoto, W. Fang, and S. Tanaka, Design and fabrication of non-resonant PZT MEMS micromirror with buried piezoresistors for closed loop position control, J. Micromech. Microeng. **33**, 014001 (2023).
4 F. Shi, N. Fantuzzi, P. Trovalusci, Y. Li, and Z. Wei, The effects of dilatancy in composite assemblies as micropolar continua, Compos. Struct. **276**, 114500 (2021).
5 B. Alemi, and H. M. Shodja, Effective moduli and characteristic lengths of micropolar media with dense periodic distribution of ellipsoidal nano-/micro-inhomogeneities, Eur. J. Mech.-A Solids **85**, 104103 (2021).
6 S. A. Ghasabi, M. Arbabtafti, and M. Shahgholi, Forced oscillations and stability analysis of a nonlinear micro-rotating shaft incorporating a non-classical theory, Acta Mech. Sin. **34**, 970 (2018).
7 S. H. Sargsyan, and M. V. Khachatryan, Construction of a bending model of micropolar elastic thin beams with a circular axis and its implementation using the finite element method, J Appl Mech Tech Phy **63**, 1205 (2022).
8 Z. He, H. Zhu, X. Wang, and S. Ma, Experimental investigation on scale effect of mechanical properties of heterogeneous micropolar medium materials, Compos. Struct. **251**, 112667 (2020).
9 A. C. Eringen, Linear theory of micropolar viscoelasticity, Int. J. Eng. Sci. **5**, 191 (1967).
10 A. C. Eringen, Theory of micropolar plates, J. Appl. Math. Phys. (ZAMP) **18**, 12 (1967).
11 A. H. Sargsyan, and S. H. Sargsyan, Natural vibrations of micropolar elastic flexible plates and shallow shells, Acoust. Phys. **68**, 118 (2022).
12 C. Zhu, C. Peng, and W. Wu, Applications of micropolar SPH in geomechanics, Acta Geotech. **16**, 2355 (2021).
13 S. Grbčić, G. Jelenić, and D. Ribarić, Quadrilateral 2D linked-interpolation finite elements for micropolar continuum, Acta Mech. Sin. **35**, 1001 (2019).
14 K. Berkache, S. Phani, and J. F. Ganghoffer, Micropolar effects on the effective elastic properties and elastic fracture toughness of planar lattices, Eur. J. Mech.-A Solids **93**, 104489 (2022).
15 Y. M. Grigor'ev, and A. A. Gavrilieva, An equilibrium of a micropolar elastic rectangle with mixed boundary conditions, Continuum Mech. Thermodyn. **31**, 1699 (2019).
16 V. A. Levin, L. M. Zubov, and K. M. Zingerman, An exact solution to the problem of biaxial loading of a micropolar elastic plate made by joining two prestrained arc-shaped layers under large strains, Eur. J. Mech.-A Solids **88**, 104237 (2021).
17 A. V. Matrosov, An exact analytical solution for a free-supported micropolar rectangle by the method of initial functions, Z. Angew. Math. Phys. **73**, 74 (2022).
18 E. Carrera, and V. V. Zozulya, Analytical solution for the micropolar cylindrical shell: Carrera unified formulation (CUF) approach, Continuum Mech. Thermodyn. doi: 10.1007/s00161-022-01156-x (2022).
19 H. Dehbani, M. Jabbari, A. R. Khorshidvand, and M. Javadi, Two-dimensional analytical solution of micropolar magneto-thermoelasticity FGM hollow cylinder under asymmetric load (r, θ), Phys. Scr. **96**, 125720 (2021).
20 G. Rizzi, H. Khan, I. D. Ghiba, A. Madeo, and P. Neff, Analytical solution of the uniaxial extension problem for the relaxed micromorphic continuum and other generalized continua (including full derivations), Arch. Appl. Mech. **93**, 5 (2023).
21 L. Leonetti, N. Fantuzzi, P. Trovalusci, and F. Tornabene, Scale effects in orthotropic composite assemblies as micropolar continua: A comparison between weak- and strong-form finite element solutions, Materials **12**, 758 (2019).
22 N. Sachio, R. Benedict, and R. Lakes, Finite element method for orthotropic micropolar elasticity, Int. J. Eng. Sci. **22**, 319 (1984).
23 A. Melaibari, A. Wagih, and M. A. Eltaher, Experimental and numerical investigation on indentation of orthotropic microplates with finite thickness, Int. Polym. Process. **35**, 314 (2020).
24 L. Huang, H. Yuan, and H. Zhao, An FEM-based homogenization method for orthogonal lattice metamaterials within micropolar elasticity, Int. J. Mech. Sci. **238**, 107836 (2023).
25 S. Yang, and S. Liu, Free vibration property analysis of composite laminated microplates based on different hypotheses in couple stress constitutive equations, Int. J. Mult. Comp. Eng. **16**, 163 (2018).
26 E. Carrera, and V. V. Zozulya, Carrera unified formulation (CUF) for the micropolar plates and shells. I. Higher order theory, Mech. Adv. Mater. Struct. **29**, 773 (2022).
27 R. S. Kumar, and D. L. McDowell, Generalized continuum modeling of 2-D periodic cellular solids, Int. J. Solids Struct. **41**, 7399 (2004).
28 A. Bacigalupo, M. L. De Bellis, and G. Zavarise, Asymptotic homogenization approach for anisotropic micropolar modeling of periodic Cauchy materials, Comput. Methods Appl. Mech. Eng. **388**, 114201 (2022).
29 L. Steinberg, Deformation of micropolar plates of moderate thickness. Int. J. of Appl. Math. Mech. **6**, 1 (2010).
30 L. Steinberg, and R. Kvasov, Enhanced mathematical model for Cosserat plate bending, Thin-Walled Struct. **63**, 51 (2013).
31 W. X. Zhong, and X. X. Zhong, Method of separation of variables and Hamiltonian system, Numer. Methods Partial **9**, 63 (1993).
32 W. X. Zhong, and X. X. Zhong, Computational structural mechanics. Optimal control and semi-analytical method for PDE, Comput. Struct. **37**, 993 (1990).
33 W. X. Zhong, Plane elasticity in sectorial domain and the Hamiltonian system, Appl. Math. Mech. **15**, 1113 (1994).
34 W. X. Zhong, Plane elasticity problem in strip domain and Hamiltonian system. J. Dalian Univ. Technol. **4**, 373 (1991).
35 W. Yao, and H. Yang, Hamiltonian system based Saint Venant solutions for multi-layered composite plane anisotropic plates, Int. J. Solids Struct. **38**, 5807 (2001).
36 X. Xu, D. Rong, C. W. Lim, C. Yang, and Z. Zhou, An analytical symplectic approach to the vibration analysis of orthotropic graphene sheets, Acta Mech. Sin. **33**, 912 (2017).
37 Z. Qiu, and H. Xia, Symplectic perturbation series methodology for non-conservative linear Hamiltonian system with damping, Acta Mech. Sin. **37**, 983 (2021).
38 C. Xu, S. Leng, Z. Zhou, X. Xu, and Z. Deng, Accurate and straightforward symplectic approach for fracture analysis of fractional viscoelastic media, Appl. Math. Mech.-Engl. Ed. **43**, 403 (2022).
39 X. Su, E. Bai, and A. Chen, Symplectic superposition solution of free

vibration of fully clamped orthotropic rectangular thin plate on two-parameter elastic foundation, Int. J. Str. Stab. Dyn. **21**, 2150122 (2021).
40 X. Su, and E. Bai, Analytical free vibration solutions of fully free orthotropic rectangular thin plates on two-parameter elastic foundations by the symplectic superposition method, J. Vib. Control **28**, 3 (2022).
41 C. Xu, D. Rong, Z. Zhou, Z. Deng, and C. W. Lim, Vibration and buckling characteristics of cracked natural fiber reinforced composite plates with corner point-supports, Eng. Struct. **214**, 110614 (2020).
42 C. W. Lim, and X. S. Xu, Symplectic elasticity: Theory and applications, Appl. Mech. Rev. **63**, 050802 (2011).
43 J. Luo, G. Liu, and W. Zhong, Symplectic solution for three dimensional couple stress problem and its variational principle, Acta Mech. Sin.. **21**, 70 (2005).
44 S. Shaw, High frequency vibration of a rectangular micropolar beam: A dynamical analysis, Int. J. Mech. Sci. **108-109**, 83 (2016).
45 C. Xu, D. Rong, Z. Tong, Z. Zhou, J. Hu, and X. Xu, Coupled effect of in-plane magnetic field and size effect on vibration properties of the completely free double-layered nanoplate system, Phys. E-Low-dimens. Syst. NanoStruct. **108**, 215 (2019).
46 E. Providas, and M. A. Kattis, Finite element method in plane Cosserat elasticity, Comput. Struct. **80**, 2059 (2002).
47 X. S. Xu, W. X. Zhong, and H. W. Zhang, The Saint-Venant problem and principle in elasticity, Int. J. Solids Struct. **34**, 2815 (1997).
48 Q. Wu, and Q. Gao, The symplectic approach for analytical solution of micropolar plane stress problem, Int. J. Solids Struct. **264**, 112095 (2023).
49 S. Hassanpour, and G. R. Heppler, Comprehensive and easy-to-use torsion and bending theories for micropolar beams, Int. J. Mech. Sci. **114**, 71 (2016).
50 S. Hassanpour, and G. R. Heppler, in Step-by-step simplification of the micropolar elasticity theory to the couple-stress and classical elasticity theories: Proceedings of ASME International Mechanical Engineering Congress and Exposition (IMECE), Montreal, 2014.
51 B. Niu, and J. Yan, A new micromechanical approach of micropolar continuum modeling for 2-D periodic cellular material, Acta Mech. Sin. **32**, 456 (2015).
52 M. Yoder, L. Thompson, and J. Summers, Size effects in lattice structures and a comparison to micropolar elasticity, Int. J. Solids Struct. **143**, 245 (2018).

正交各向异性微极平面应力问题的辛求解方法

陈龙, 汤兆飞, 吴穹, 高强

摘要 本文采用辛弹性力学方法得到正交各向异性微极平面应力问题的解析解. 首先, 应用勒让德变换和哈密顿混合能量变分原理得到哈密顿正则方程. 然后, 利用分离变量法, 导出了相应的齐次哈密顿正则方程的本征问题. 最后, 推导了三种齐次边界条件下问题的相应本征解. 根据本征解的共轭辛正交性和展开定理, 正交各向异性微极平面应力问题的解可以表示为这些本征解的级数展开. 本文给出了各种边界条件下平面应力问题的数值结果, 并用有限元法证明了该方法的收敛性和准确性. 同时使用该方法研究了尺寸效应和材料尺度参数之间的关系. 并且, 在等效微极连续介质近似下, 使用辛方法分析格子结构的力学行为.